TO APPEAR IN APJ., XX.
Preprint typeset using LaTeX style emulateapj v. 8/13/10

MODELING DEUTERIUM FRACTIONATION IN COLD AND WARM MOLECULAR ENVIRONMENTS WITH LARGE CHEMICAL NETWORKS

T. ALBERTSSON[1], D. A. SEMENOV [1] AND TH. HENNING [1]
Max-Planck-Institut für Astronomie, Königstuhl 17, 69117 Heidelberg, Germany
To appear in ApJ., xx.

ABSTRACT

Observations of deuterated species have long proven essential to probe properties and thermal history of various astrophysical environments. We present an elaborated chemical model that includes tens of thousands of reactions with multi-deuterated species, both gas-phase and surface, in which the most recent information on deuterium chemistry is implemented. A detailed study of the chemical evolution under wide range of temperatures and densities typical of cold molecular cores, warm protostellar envelopes, and hot cores/corinos is performed. We consider two cases of initial abundances, with 1) mainly atomic composition and all deuterium locked in HD, and 2) molecular abundances accumulated at 1 Myr of the evolution of a cold prestellar core. We indicate deuterated species that are particularly sensitive to temperature gradients and initial chemical composition. Many multiply-deuterated species produced at 10 K by exothermic ion-molecule chemistry retain large abundances even when temperature rises above 100 K, and can only be destroyed by dissociation. Our model successfully explains observed D/H ratios of many single, double, and triple-deuterated molecules, including water, methanol, ammonia, and hydrocarbons in a variety of environments (cold cores, hot protostellar envelopes and hot cores/corinos). We list the most abundant deuterated species predicted by our model in different environments of low- and high-mass star-formation regions, as well as key formation and destruction pathways for DCO^+, DCN and isotopologues of H_2O, H_3^+ and CH_3OH.

Subject headings: astrochemistry – molecular processes – methods: numerical – ISM: clouds, molecules – stars: circumstellar matter, protostars

1. INTRODUCTION

The life cycle of molecules covers a wide range of environments in the evolution of gas and dust, beginning from the sparse interstellar medium and eventually evolving into stars, planets and possibly life itself. Molecular hydrogen cannot be easily observed in the cold interstellar medium, therefore, we have to use other atomic and molecular tracers. The study of deuterium chemistry has proven to be useful to constrain ionization fraction, temperature, density, and thermal history of the interstellar medium (ISM) (Geiss & Reeves 1981; Turner 1990; Crapsi et al. 2005).

More than 160 molecules have to date been observed in the interstellar medium, identified using radio and infrared observations of their rotational and rovibrational transitions. The detected molecules include singly- and multi-deuterated species that have been observed in molecular clouds (ND; Bacmann et al. 2010), (DCO^+, DNC; van der Tak et al. 2009), hot cores/corinos (D_2CO, HDCO; Bergman et al. 2011), (HD_2^+; Vastel et al. 2004), ($DCOOCH_3$; Demyk et al. 2010; Margulès et al. 2010), warm protostellar envelopes (HDO; Jørgensen & van Dishoeck 2010; Liu et al. 2011), (DCO^+, HDCO; Parise et al. 2009), protoplanetary disks (HDO; Qi et al. 2008; Ceccarelli et al. 2005), (DCN, DCO^+; Guilloteau et al. 2006; Qi et al. 2008), and comets (HDCO; Kuan et al. 2008), (HDO; Villanueva et al. 2009; Gibb et al. 2010), (CH_3D; Bonev et al. 2009; Gibb et al. 2010). Many deuterated species remain however elusive due to their low abundances and/or weak transitions. With the completion of the sensitive Atacama Large Millimeter Array (ALMA) we will be able for the first time to detect and probe various astrophysical environments in weak lines of numerous complex and rare-isotope molecules, including multi-deuterated species.

Yet, in order to understand the observations of these molecules, feasible models and state-of-the-art chemical networks have to be utilized. Detailed theoretical studies of deuterium chemistry is difficult due to the limited number of known reactions rates involving deuterated species, and a vast amount of hydrogen-dominated reactions. Previous studies either made due with what available data there were, or using "educated guesses" for missing reaction rates (e.g., Rodgers & Millar 1996; Turner 2001; Aikawa et al. 2003). Also, often deuterated species with only one or two D-atoms have been considered. First studies of deuterium chemistry included only a limited amount of reactions due to restricted computer power, such as the one adopted by Brown et al. (1988), including 93 species connected by 703 reactions. Results were accompanied with large errors, but over time the size of the chemical networks have increased significantly, and with it the level at which we can understand the complexity of the chemical evolution in the interstellar medium.

The isotopologues of H_3^+ have been known for a long time to play a key role in deuterium fractionation in cold environments, together with other associated ions such as DCO^+ and H_2DO^+. The chemical evolution of H_2D^+ and the other isotopologues have been found to be closely linked to CO, acting as the main destruction path (Bacmann 2003). This leaves room for other species to dominate deuterium fractionation in warmer environments, such as CH_2D^+ and C_2HD^+ (Millar et al. 1989).

The importance of H_3^+ on the efficiency of the deuterium fractionation via gas-phase chemistry has been investigated by Roberts et al. (2003). They have found that in regions of high density and heavy depletion, which is the case in prestellar cores, inclusion of isotopologues of H_3^+ significantly enhanced the fractionation of ionic and neutral species. Other studies have been done, also proving the importance of the isotopologues of H_3^+, such as Roberts et al. (2003), Roberts

& Millar (2006) and van der Tak (2006).

As Roberts et al. (2003) have found, the environment plays an over important role in the chemical evolution. Roberts & Millar (2000b) have studied the chemistry a wide range of physical parameters, varying density, temperature, initial abundances and freeze-out of molecules. They have found that fractionation is strongly affected by temperature, and agreed reasonably well with the limited data on sulfur-bearing species observed in dark clouds. If freeze-out is present, molecular D/H ratios can become very high, and gas-phase chemistry can result in very large abundances of both singly- and multi-deuterated molecules.

Willacy (2007) and Willacy & Woods (2009) have studied the deuterium chemistry in the outer and inner regions of protoplanetary disks, and found that in the outer regions, photodesorption is essential in the midplane for high abundances of molecules such as HDO, and that the DCO^+ fractionation ratio is very sensitive to what desorption mechanism is implemented. In the inner regions, they found their calculated D/H ratios on ices to be too high compared to observations of comets, which suggests that the model is incomplete, possibly lacking essential surface reactions. Their results are quite different compared to older study of Aikawa & Herbst (1999). Aikawa & Herbst have found that their chemical model reproduces higher than cosmic D/H ratios in disks, as observed in comets, and that the D/H ratio is sensitive to the adopted thermal and ionization disk structure, regulating D-fractionation via ion-molecule chemistry. Bayet et al. (2010) have conducted a survey of deuterated species in extragalactic star-forming regions, studying the influence of density, temperature, far-UV radiation field, cosmic-ray ionization and metallicity on D/H ratios of about 20 deuterated species. Their results agree well with the limited observations in external galaxies, and provide a list of key deuterated species whose abundances are high enough to possibly be detected by Herschel and ALMA.

The surface chemistry on grains have recently been implemented into chemical models, as their importance has been unveiled as crucial catalysts for complex organics (Herbst & van Dishoeck 2009), and other molecules such as H_2 and water. Although having a profound effect on the evolution of molecules, it remains poorly understood. Extensive laboratory studies have investigated the importance of surfaces in deuterium chemistry (e.g., Hidaka et al. 2006; Nagaoka et al. 2006), as well as theoretical studies (e.g., Watanabe 2005; Cazaux et al. 2008; Kalvans & Shmeld 2011). As hydrogen- and deuterium-bearing molecules are destroyed at approximately the same rates, Rodgers & Millar (1996) have found that initial high D-fractionation in ice mantles can persist for over 10^4 years, which holds true for a wide range of physical conditions. This means that it is safe to infer fractionation on grains from observations of deuterated molecules in hot cores.

The Herschel observatory is currently gathering measurements (e.g., Vastel et al. 2010; Comito et al. 2010; Bacmann et al. 2010), and with the upcoming ALMA, SKA, and JWST facilities, the interest in deuterium chemistry will only grow. In the advent of the high-sensitivity, high-resolution measurements these facilities will contribute, we have conducted an extensive study of deuterium chemistry in both cold and hot molecular environments shielded from ionizing radiation by the A_V extinction of 10 mag. The main aim of the present study is to investigate qualitatively and quantitatively deuterium fractionation and chemical evolution for an extended set of diagnostic species, ranging from simple mono-deuterated molecules to triple-deuterated complex organics, using a newly-developed up-to-date chemical network (available online). Another motivation is to try to reproduce simultaneously observed D/H ratios of a variety of mono-, doubly-, and triply-deuterated species in distinct astrophysical environments (e.g., $HDO/DCO^+/DCN$, $ND_2/D_2O/D_2CO$, and CD_3OH).

In Section 2 we present the chemical model of Semenov et al. (2010) adjusted to the ISM conditions and use it to model chemical evolution in a wide temperature-density parameter space. The parameter space represents evolutionary stages from cold, dark, low-mass clouds to the warm dense medium in hot cores/corinos (Section 2.1). We give a detailed description of the deuterium cloning process and our choice of mass-dependent fractionation reaction rates and branching ratios of relevant dissociation reactions in Section 2.3. In Section 3 this model is used to calculate chemical abundances and D/H ratios for assorted species. The general trends as well as detailed evolution of assorted species are analyzed in Sections 3.1 and 3.2. We compare our results with recent observations and theoretical studies in Discussion. Summary and Conclusions follow.

2. MODEL

2.1. *Physical model*

Deuterated species have been observed extensively in varieties of astronomical objects located locally in the Galaxy and at high-z redshifts. In this work we are primarily concerned with modeling deuterium chemistry in cold low-mass prestellar cores and warm/hot high/low-mass cores and corinos. The evolution of the interstellar medium begins from fragmentation of turbulent, partly molecular, partly atomic clouds, having temperatures of about 80 K and low densities of ~ 10 cm^{-3}. Eventually some of the clumps form prestellar cores having low temperatures of 8-15 K and moderate densities, $\sim 10^4 - 10^6$ cm^{-3} (Launhardt et al. 2010; André et al. 2009; Snow & McCall 2006), which is favorable for accumulating high degrees of deuterium fractionation enabled by the ion-molecule chemistry via H_3^+ isotopologues. Eventually some clouds begin contracting due to gravitation, increasing internal densities and temperatures. Then a protostar is born, which begins to heat up its surroundings. The envelope material can then reach temperatures $\gtrsim 100$ K with densities $\lesssim 10^{10}$ cm^{-3} (van Dishoeck 2009). The protostellar environment then evolves into a protoplanetary disk, which is heavily irradiated by the stellar FUV and X-ray radiation, and later a planetary system.

In this paper we will concentrate on the evolutionary stages ranging from a cold molecular cloud to a hot core, discarding the later evolutionary stages. We intentionally choose a wide parameter space covering temperatures between 5 - 150 K and densities of 10^1 - 10^{10} cm^{-3}, assuming fixed A_v = 10 mag (for the standard ISM dust). That is, our study is focused on heavily obscured regions of the ISM and dark protoplanetary disk midplanes. The simulations with the fixed extinction allow us to plot the respective abundances and D/H ratios as 2D plots, which are easier to interpret and discern general trends.

2.2. *Chemical model*

We have utilized the gas-grain chemical model "ALCHEMIC" developed by Semenov et al. (2010), where detailed description of the code and performance is avail-

able. The code is optimized for time-dependent evolution of large chemical networks including both gas-phase and surface species. A brief summary is given below.

The chemical network is based on the osu.2009 ratefile with the recent updates to reaction rates as of Nov 2010[1]. Several tens of photoreaction rates are updated using the new calculations of van Dishoeck et al. (2006), which are publicly available[2]. The self-shielding of H_2 from photodissociation is calculated by Equation (37) from van Dishoeck & Blake (1998). The shielding of CO by dust grains, H_2, and its self-shielding is calculated using the precomputed table of Lee et al. (1996, Table 11).

We consider cosmic rays (CRP) as the only external ionizing source (as well as CRP-induced FUV photons), using the standard CRP ionization rate, ζ_{CR} = 1.3 x 10^{-17} s^{-1}. The gas-grain interactions include sticking of neutral species and electrons to uniformly-sized 0.1 μm dust grains with a sticking coefficient of 1, release of ices by thermal, CRP-, and UV-induced desorption, dissociative recombination and radiative neutralization of ions on charged grains, and grain recharging. We do not allow H_2 and its isotopologues sticking to grains. Chemisorption of surface molecules is also not considered. We assume the UV photodesorption yield of 10^{-3} (e.g., Öberg et al. 2009a,b,c). To allow synthesis of complex molecules, an extended list of surface reactions and photodissociation of ices is adopted from Garrod & Herbst (2006).

We assume that each 0.1μm spherical olivine grain provides $\approx$ 2 x 10^6 sites for surface recombination that proceeds solely through the Langmuir-Hinshelwood mechanism. Upon a surface recombination, there is a 5% chance for the products to leave the grain due to release of energy. Following experimental studies on the formation of molecular hydrogen on dust grains by Katz et al. (1999), we adopt the standard rate equation approach to the surface chemistry without quantum-mechanical tunneling either through the potential walls of the surface sites or through the reaction barriers.

A typical run, with relative and absolute accuracies of 10^{-5} and 10^{-15}, the full gas-grain network without deuterium chemistry ($\sim$ 7000 reactions, $\sim$ 650 species) takes a few seconds for 5 Myr of evolution (Xeon 2.8GHz CPU). The same model with added deuterium chemistry ($\sim$ 52,000 reactions and $\sim$ 1,700 species) takes approximately an order of magnitude longer to calculate.

2.3. *Deuterium chemistry*

As we aim to conduct an extensive deuterium chemical network, we have followed the same algorithm as described in Rodgers & Millar (1996). Namely, reactions bearing hydrogen atoms are considered to have deuterated analogues, and "cloned" accordingly (assuming the same rate coefficient if no lab data are available). In cases where the position of the deuterium atom is ambiguous, we apply branching ratios, dividing the total rate coefficient over the number of reaction channels.

In Equation (1) a typical example of the cloning process is presented, which results in three separate reactions depending on where the deuterium is placed. The original reaction is to the left, and to the right are the three possible isotopic pathways, each with a branching ratios of 1/3.

$$C_4H_2^+ + S \rightarrow HC_4S^+ + H \Rightarrow \begin{cases} C_4HD^+ + S \rightarrow DC_4S^+ + H \\ C_4HD^+ + S \rightarrow HC_4S^+ + D \\ C_4D_2^+ + S \rightarrow DC_4S^+ + D \end{cases} \quad (1)$$

A few restrictions are applied to the cloning routine. Due to the significantly large number of hydrocarbons in the network, species with more than six chained carbon atoms (C6-) are not isotopically cloned. Any -OH endgroups are conserved as well. Observations of deuterated species suggest that fractionation of species with -OD endgroups is less probable and can be excluded. For example, Parise et al. (2006) have conducted a survey of deuterated formaldehyde and methanol, and found that the fractionation level of CH_3OD is at least an order of magnitude lower than that of CH_2DOH. A hypothesis of rapid conversion of CH_3OD into CH_3OH in the gas-phase due to protonation reactions that would affect only species for which deuterium is bound to the electronegative oxygen has been suggested by Osamura et al. (2004); Charnley et al. (1997), which further support this.

This method is applied to the latest osu.2009 chemical network, excluding the recently added fluorine reactions, and including updated rate coefficients from Roberts & Millar (2000b); Roberts et al. (2004); Wakelam et al. (2010); Chabot et al. (2010) as well as from the KInetic Database for Astrochemistry[3]. Isotope exchange reactions involving all isotopologues of H_3^+ as well as CH_2D^+, C_2HD^+ and others have been taken from Roberts & Millar (2000b) and Roberts et al. (2004).

A table of added and updated reactions are listed in Tables A1 and A2. This has resulted in a chemical network consisting of 52,548 reactions connected by 1,716 species, to our knowledge the most extended network for deuterium chemistry to date.

2.4. *Initial abundances*

Reaction rates and physical properties need to be specified for the model, as does initial abundances. We have chosen to implement two different initial abundances and investigate how they affect the chemical evolution over 1 Myr under considered parameter space. In both models, all deuterium is initially located in HD, with D/H = 1.5 x 10^{-5} (Stancil et al. 1998; Linsky 2003). This is valid as the zero-point energies of HD and H_2 differ by $\sim$ 410 K, hence favoring production of HD over H_2(Roberts et al. 2003).

For the first model, hence on referred to as the "Primordial" model, we utilized "low metals" abundances of Lee et al. (1998), supplied with the HD abundance of 1.5×10^{-5} (Table 1). The initial abundances for the second model, the "Evolution" model, are calculated with our deuterium chemistry model using a TMC-1 environment: T = 10 K and $n_H = 10^4$ cm^{-3}, for 1 Myrs. Under such conditions deuterium fractionation becomes very effective, leading to high fractionation levels for many species. The final TMC-1 abundances at 1 Myr are used as initial abundances for the "Evolution" model. The most abundant deuterated species are given in Table 2.

3. RESULTS

We study the general trends of the fractionation ratios of deuterated species, looking at dependencies on temperature,

[1] See: http://kida.obs.u-bordeaux1.fr

[2] http://www.strw.leidenuniv.nl/~ewine/photo/

[3] http://kida.obs.u-bordeaux1.fr/ as of [2010-12-20]

Table 1
Initial abundances for the Primordial model.

Species	H_2	H	HD	He	C	N	O
	0.499	2.00×10^{-3}	1.50×10^{-5}	9.75×10^{-2}	7.86×10^{-5}	2.47×10^{-5}	1.80×10^{-4}
	S	Si	Na	Mg	Fe	P	Cl
	9.14×10^{-8}	9.74×10^{-9}	2.25×10^{-9}	1.09×10^{-8}	2.74×10^{-9}	2.16×10^{-10}	1.00×10^{-9}

Table 2
Initial abundances for the Evolution model.

Species	H_2	H	HD	He	C	N	O
	0.500	1.54×10^{-4}	5.26×10^{-6}	9.75×10^{-2}	6.05×10^{-9}	9.18×10^{-8}	8.55×10^{-7}
Species	S	Si	Na	Mg	Fe	P	Cl
	3.13×10^{-9}	1.05×10^{-10}	8.64×10^{-11}	4.10×10^{-10}	6.36×10^{-11}	1.09×10^{-11}	1.43×10^{-10}
Species	D	D_2	HDO (ice)	CH_3D (ice)	OD	NH_2D (ice)	CH_3D
	4.20×10^{-6}	1.86×10^{-6}	8.64×10^{-7}	3.54×10^{-7}	1.27×10^{-7}	1.26×10^{-7}	5.01×10^{-8}

density and initial abundance. We also do in-depth studies of several assorted species representing certain groups of molecules including ions, complex molecules as well as important molecular probes.

3.1. *General trends*

Plots of the D/H fractionation ratios for both chemical models and assorted species are shown in Figure 1. The left panel in each subplot is the *Primordial* model and the *Evolution* model is shown in the right panel. Species in the four topmost subplots show mainly dependence on the initial abundance, with differences in fractionation ratios between the models at $T \gtrsim 40-50$ K. The middle four plots mainly show dependence on temperature, and no dependence on the initial abundance. The last four subplots show D/H ratios that are sensitive to neither the kinetic temperature or the initial abundances. Assorted molecules distributed in these three distinct groups are listed in Table 3.

The computed D/H fractionation ratios reach levels of $\sim 10^{-3}$ and higher for most of species, which is an enhancement by ~ 2 orders of magnitude relative to the cosmic D/H ($\sim 1.5 \times 10^{-5}$). Only at $T \gtrsim 100$ K do the ratios reach the low cosmic values for some of the molecules. Observationally this overabundance, primarily in cold environments, has been found for many deuterated species. For example, the observed abundances are $> 10\%$ of their main isotopologues for species such as CH_2DOH, D_2CO (Ceccarelli 2002), D_2O (Butner et al. 2007), H_2D^+ (Caselli et al. 2003), HDO (Liu et al. 2011) and NH_2D (Hatchell 2003), etc. We discuss the comparison of observations with our models further in Section 4.1. So far no unique solution has been found to explain these deuterium enhancements, though usually either gas-phase or grain-surface fractionation routes have been invoked (e.g., Roberts et al. 2004; Charnley et al. 1997).

The deuterated species are affected differently by variations in temperature and the initial abundances. While kinetic temperature is a key factor for mass-dependent fractionation processes, the choice of initial abundances is also important to retain certain level of pristine fractionation accumulated at low temperatures even when $T \gtrsim 50-100$ K. The sensitivity of the D/H ratios to density is, in general, weak since most of the chemical reaction rates for main and minor isotopologues of a chemical species will be similar. The only exception is light-weight multi-deuterated species like D_2, H_2D^+, D_2H^+, etc., having the largest mass differences with their major isotopologues, and thus the largest deviation in their desorption and surface reaction rates. It is, perhaps, most evident for H_2D^+, shown in Figure 1, and the other minor isotopologues of H_3^+. These species experience a drop in fractionation ratios toward lower densities, however only visible towards low temperatures. For species that are strongly dependent on the production of the H_3^+ isotopologues, the same dependence is noticeable, however somewhat diluted by a larger number of intermediate reactions. This can be understood as a manifestation of the unique role of mass-fractionation relevant for deuterium chemistry, which is solely dependent on gas temperature and barely on its density. Therefore we do not treat density dependence separately but rather discuss it together with the other parameters.

The majority of species show strong dependency on the initial abundances, somewhat fewer strictly to temperature and even less, such as CH_3D, CHDCO and HDCS, show no dependency both either parameter. Freeze-out species barely show any difference in the distribution of fractionation ratios compared to the gas-phase molecules, so generally the same general trends apply for species on grains.

In the "Primordial" model, for species dependent on the initial abundance, the D/H fractionation ratios can drop several orders of magnitude at higher temperatures ($T \gtrsim 50-80$ K), down to the cosmic value, while in the "Evolution" model they usually remain almost as high as in cold environments, with only local drops and enhancements. Most radicals are strongly sensitive to the choice of the initial abundances, and only a few of them show a strict sensitivity to temperature, such as DCN and CD_2CO. Another group of species systematically showing strong dependence on the initial abundances are multi-deuterated species. Ions, however, show stronger dependency on the gas temperature, as their chemical evolution is closely related to that of isotopologues of H_3^+. Only a small number of ions are dependent on the initial abundances, such as DCO^+ and N_2D^+.

3.1.1. *Sensitivity of D/H to the initial abundances*

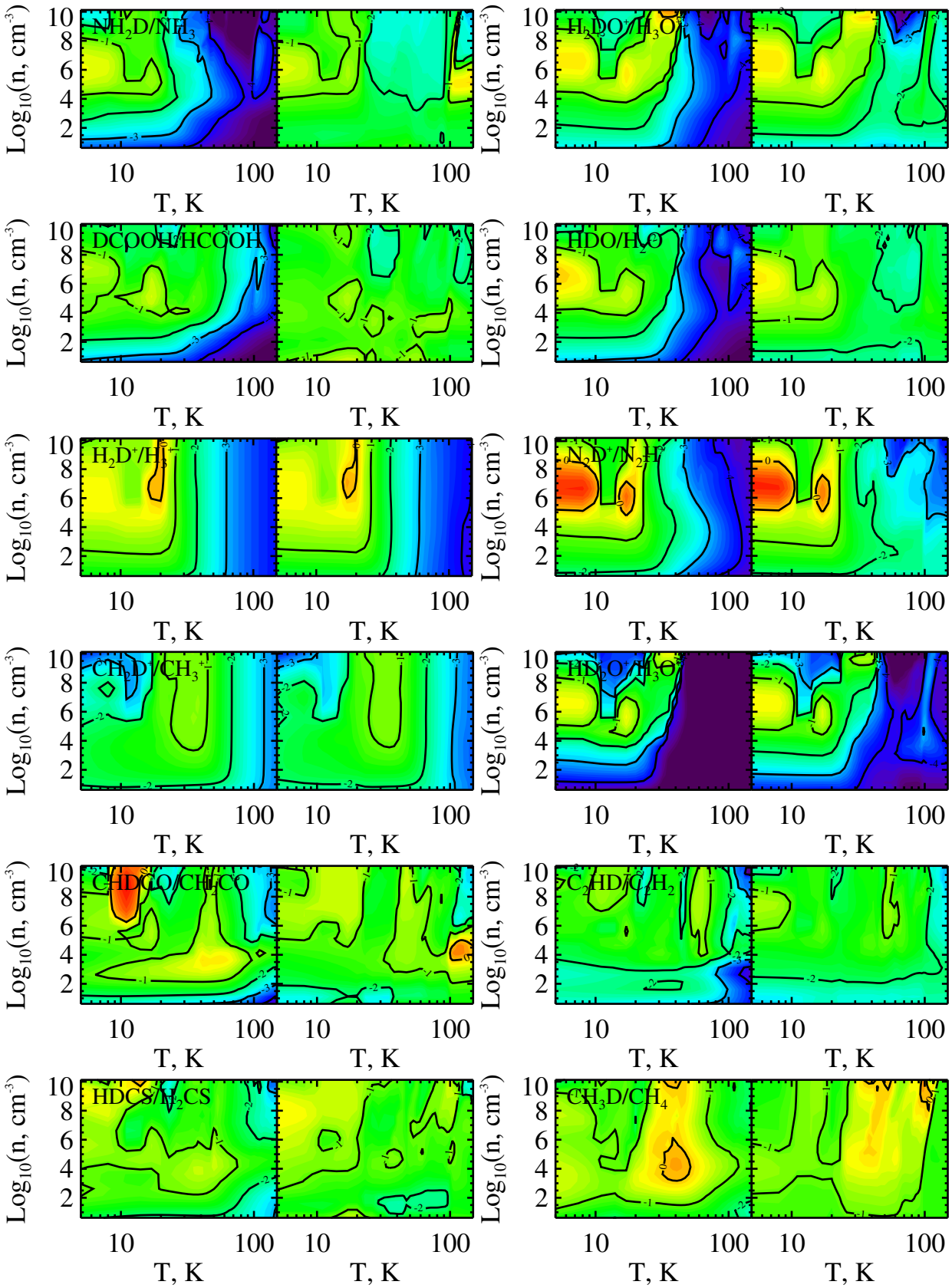

Figure 1. Plots of the D/H ratios at 1 Myr for the "Primordial" (left) and "Evolution" (right) models showing different dependencies to physical parameters and the initial abundances. The species are (left to right): NH_2D, H_2DO^+, DCOOH, HDO, D_2O, H_2D^+, N_2D^+, CH_2D^+, CHDCO, C_2HD, HDCS, CH_3D.

Table 3
Species showing dependence on initial abundance, temperature or independent to both.

Initial abundance dependence	Temperature dependence		Independent
	Low	High	
C_2D, C_2HD, C_3HD, C_4D, C_4HD, CD_3OH	C_2D_2, CD_3^+	$C_2D_2^+$, C_2HD^+	C_3H_3D, CH_3D, CHDCO
CD_4, CD, CH_2D_2, CH_2DOH, CHD_2OH, CHD_3	CHD_2^+, D_3^+	CD_2CO, CH_2D^+	D_2, CD (ice), HDCS, HD
D_2CS, D_2O, D_2S, DC_3N, DC_5N, DCO^+	D_3O^+, DCN	H_2D^+	
$DCOOCH_3$, DCOOD, DCOOH, DNC, DNCO, DNO	HD_2^+		
DOC^+, H_2DO^+, HD_2O^+, HDCO, HDO, HDS, N_2D^+			
ND_3, ND, NH_2D, NHD_2, OD			

The initial abundances are bound to have a great effect on many species, as the abundances of molecules initially present in the "Evolution" model allow for deuterated and more complex molecules to begin forming much faster, and to survive for much longer at elevated temperatures. In Figure 1, the top four species show strong dependence on the initial abundance, as the two models show significantly different distributions of fractionation ratios, in particular, at high temperatures. For many species, the "Evolution" model has close to a uniform distribution of fractionation ratios of $\gtrsim 10^{-3}$, while "Primordial" models show a significant drop toward higher temperatures ($\gtrsim 100$ K).

Species are affected differently by changes in the physical parameters due to the pace at which they are produced, destroyed, accreted, and evaporated. This in turn is determined by the number of reaction pathways, their reaction rates, and how many intermediate molecules their formation is dependent on. In the "Primordial" model, there are initially only the basic elements present, along with H_2 and HD, which, as soon as the simulations begin, are redistributed to form new species of increasing chemical complexity. The adopted low $T = 10$ K in this model results in efficient deuterium fractionation via ion-molecule chemistry driven by the D-isotopologues of H_3^+ initially, and other channels later (neutral-neutral gas-phase and surface reactions). The reverse processes in this case typically imply substantial reaction barriers ($\gtrsim 500-1\,000$ K) to reach the cosmic D/H abundance values. Consequently, the "Evolution" model starts with complex molecules, including a large fraction of overabundant deuterated species, that may retain their abundances even at $T > 100$ K. Therefore, "Primordial" model show big differences compared to the "Evolution" model, especially, at $T \gtrsim 50$ K. A vast majority of the species dependent to the initial abundance are radicals, spreading between combinations of H, C, O and S-bearing species, up to complex organics. A small number of key ions are also found in this group: DCO^+, DOC^+, N_2D^+, H_2DO^+ and HD_2O^+.

In Figure 2, we show a few example of multi-deuterated species sensitive to the initial abundance. Multi-deuterated species are formed in a long chain of formation and D-fractionation channels, causing the production speed to be slow. In the "Primordial" model there are none of the preceding species present initially, and producing multi-deuterated species becomes time-consuming. In the "Evolution" model, in contrast, the preceding deuterated species can be present in large amounts to start forming even more complex multi-deuterated species early on during the evolution. Therefore, many of the multi-deuterated species have different distributions of the D-fractionation ratios between the two models.

3.1.2. *Sensitivity of the D/H ratios to temperature*

A number of species shows dependency on temperature, without any significant differences between the two models of initial abundances (see Figure 1, middle four plots). At temperatures exceeding about $20-50$ K, the fractionation ratios drop, either abruptly, or smoothly, and both models show a similar gradient with temperature. These dependencies trace back to either one or several dominant chemical channels being activated at certain temperatures, decreasing the abundance of the deuterated species or slowing down the production.

Ions represent a majority of the species dependent strictly on temperature, although the most common ions are dependent on the initial abundances. The best example of such species is H_2D^+, shown in Figure 1, and the other isotopologues of H_3^+. It shows a strict barrier with a temperature of 20 K, after which the fractionation ratios drop smoothly and reach levels comparable to the cosmic level ($\sim 10^{-5}$) at about 100 K. We present further discussion of the evolution of the isotopologues of H_3^+ in Section 3.2.1.

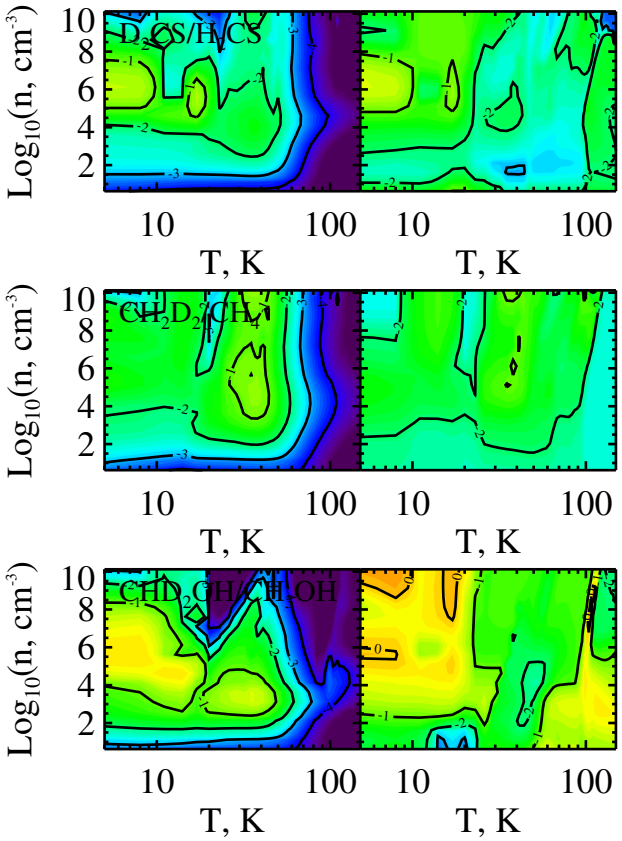

Figure 2. Plots of the D/H ratios at 1 Myr for the "Primordial" (left) and "Evolution" (right) models for assorted multi-deuterated species showing dependence on the initial abundances. The species are (left to right): D_2CS, CH_2D_2 and CHD_2OH.

This group of species with strict dependency on temperature can be split into two subgroups, diverging by the critical temperature where the D/H ratios begin to decrease. The deuterated species formed via low-temperature fractionation channels involving isotopologues of H_3^+ have a critical temperature of ~ 40 K, whereas other D-species synthesized via high-temperature fractionation channels involving CH_2D^+ and C_2HD^+ show higher critical temperature of ~ 80 K (Parise et al. 2009). Several multi-deuterated species belong exclusively to the low-temperature group.

3.2. *Detailed chemical analysis for assorted species*

We have looked more thoroughly at a selection of species, chosen by their importance as representatives of different groups of molecules. Among the selected species, we have representative ions (isotopologues of H_3^+, DCO^+), simple molecules (DCN), complex organics (isotopologues of CH_3OH) and water (HDO, D_2O), which is gaining a lot of interest now with Herschel observations and the upcoming ALMA facility.

We analyze the evolution of these representative species in four distinct astrophysical environments: densities of 10^4 and 10^8 cm^{-3}, and temperatures of 10 and 80 K for the "Primordial" and "Evolution" models. Using our robust "Chemical

Analyzer" (CHAN) tool, we isolate the most important formation and destruction pathways for each of these species. Pathways are considered dominant if they contribute to at least 10% of the net abundance change. Reactions with branching ratios are considered important when their combined rate contributes to $\gtrsim$ 10% of the net abundance change. We list key formation and destruction pathways for the assorted species and their main reactants in Table B1, B2, B3, B4, B5 and B6, and discuss their formation briefly below.

3.2.1. H_3^+ *isotopologues*

The isotopologues of H_3^+ have been a target of extensive investigation, most recently by, among others, Roberts & Millar (2006), Sipilä et al. (2010); Vastel (2007); Vastel et al. (2006b); van der Tak (2006), and Roberts et al. (2003). There is a large interest in these isotopologues as they serve as excellent probes of physical properties of the interstellar medium, and as the starting point for ion-molecule chemistry. The formation of the H_3^+ isotopologues is believed to be well understood, formed through ongoing deuteration of H_3^+ and its isotopologues by reacting with HD. H_3^+ is formed through H_2^+, which is formed by cosmic rays ionizing molecular hydrogen. Key formation and destruction pathways are summarized in Table B1, and for essential reactants in Table B2, but essentially formation proceeds as follows:

$$H_2 + h\nu \Rightarrow H_2^+ \quad (2)$$
$$H_2^+ + H_2 \Rightarrow H_3^+ \quad (3)$$
$$H_3^+ + HD \Rightarrow H_2D^+ + H_2 \quad (4)$$
$$H_2D^+ + HD \Rightarrow HD_2^+ + H_2 \quad (5)$$
$$HD_2^+ + HD \Rightarrow D_3^+ + H_2 \quad (6)$$

The isotopologues have been observed extensively; e.g. H_2D^+ (Caselli et al. 2008; Cernicharo et al. 2007; Harju et al. 2006) and HD_2^+ (Parise et al. 2011; Vastel et al. 2004). While observations of the ortho- or para-states of these isotopologues have been successful, we have not considered it in our models. The fully deuterated D_3^+ is symmetric and not observable in the sub-mm range, and the same goes for H_3^+, making it hard to determine fractionation ratios for the species directly. H_3^+ can instead be measured using IR/optical absorption of its electronic transition toward warm environments (Goto et al. 2008).

All the H_3^+ isotopologues show dependence on temperature, and partly on density, as can be seen in Figure 3. In general, the fractionation ratios reach values above 10^{-3}, and only at temperatures above $\sim$ 30 K does it go lower. The decrease is noticeable as a clear fractionation boundary towards the higher temperatures, which is more pronounced for the multi-deuterated isotopes. At lower temperatures there is weak dependency on density, with higher fractionation ratios achieved toward higher densities.

D_3^+ show significantly higher D/H fractionation ratios at low temperatures, increasing with density, up to values as high as $10-20$, while other H_3^+ isotopologues reach values of $10^{-1}-1$ at most. At $T \lesssim 20$ K, backward de-fractionation reactions are not active, and fractionation goes fast because the main destruction channel via the ion-molecule reaction with CO is absent due to all CO being locked in grain icy mantles (Vastel et al. 2006b; Bacmann et al. 2003). Since the energy barriers of the backward reactions cannot be overcome, and D_3^+ cannot be further deuterated, it will be a final product of the H_3^+ fractionation, and thus it reaches the highest D/H fractionation compared to those of HD_2^+ and H_2D^+.

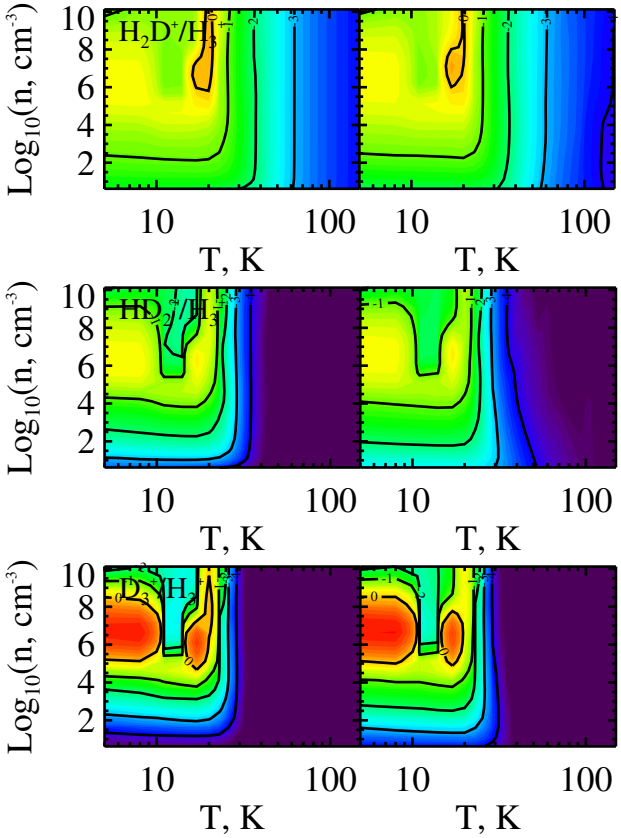

Figure 3. Distribution of the D/H fractionation ratios over the investigated parameter space, for the three isotopologues of H_3^+ and the two sets of the initial abundances.

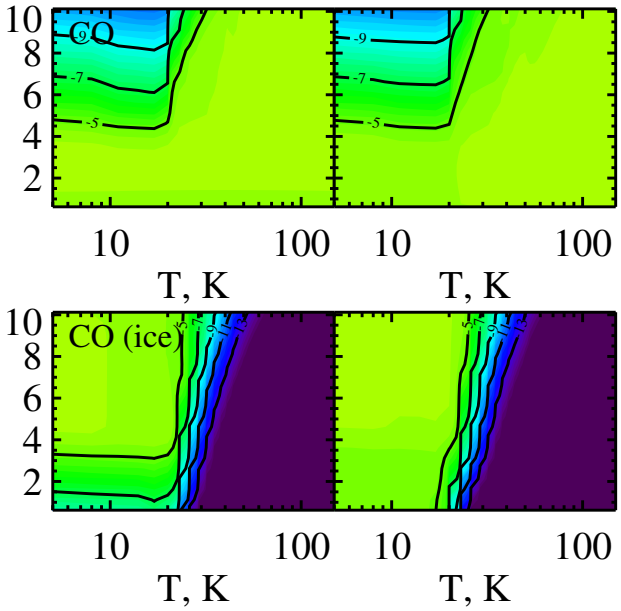

Figure 4. Relative abundances at 1 Myr of the CO molecule, both in gas-phase and ices for the "Primordial" (left panel) and "Evolution" (right panel) models.

In the limit where CO is depleted onto grains at T $\lesssim$ 20 K (see Figure 4), D_3^+ can theoretically reach values $\sim$ 20, while

H_2^+ and HD_2^+ reach levels of unity (Roberts 2005), which is in agreement with our results. Finally, the drop of the D/H ratios for the H_3^+ isotopologues observed in Figure 3 at densities exceeding 10^8 cm^{-3} is due to steady removal of the elemental deuterium in the gas-phase in deuterated ices, such as HDO, D_2O, CH_3D, NH_2D, etc., by surface processes. This reduces the pace of the deuterium fractionation via H_3^+ as abundances of HD and other gas-phase D-species go down, whereas abundances of H_3^+ increase, thus decreasing the corresponding D/H ratios. Long timescales associated with these surface processes require high densities to have profound effect on the H_3^+ abundances during the 1 Myr evolutionary time span.

An area of high D/H at $\sim$ 20 K, towards densities above $\sim 10^6$ cm^{-3}, is present for all the H_3^+ isotopologues, which we will refer to as fractionation "islands". Two big nearby peaks are evident that reach D/H close to or above unity, especially evident for D_3^+. As we discussed above, this is due to extreme molecular depletion of major destruction agent for the H_3^+ isotopologues, namely the CO gas, and the evolution becomes restricted to a limited set of reactions. Under these circumstances, the network becomes bistable to slight changes, because a certain species may be more/less depleted than others. Therefore, it is merely a feature of our model, and since the isotopologue radicals are highly reactive, acting as starting point for the formation of many molecule, it will affect the distribution of other deuterated species as well.

3.2.2. *H_2O isotopologues*

Water is one of the most essential molecule in the context of planet habitability and the evolution of complex lifeforms, and is gaining a lot of interest in the light of results on exoplanets from Kepler, as well as the Herschel results and in light of upcoming ALMA facility. A lot of effort is put on understanding the presence of water throughout the evolution of the interstellar medium and protoplanetary disks. In this context, we perform a deeper analysis of the chemical evolution of the deuterated isotopologues of water; HDO and D_2O, and deduce their main reaction pathways.

Plots of the fractionation ratios for deuterated water, both gaseous and solid, are shown in Figure 5. The highest modeled D/H ratio for HDO and D_2O is $\gtrsim$ 10%, achieved at temperatures below about 20 K and moderate densities of $10^6 - 10^8$ cm^{-3}. There are some significant differences between the two water isotopologues in the two initial abundances models. The "Primordial" model shows strong temperature dependence for the both isotopologues, although not as clear as for the isotopologues of H_3^+. None of the most dominant formation reactions for either HDO or D_2O show any temperature dependence, suggesting instead that it is inherited from the chemical evolution and fractionation efficiency of H_3^+. Table B3 lists the key formation and destruction pathways associated with the water isotopologues, mainly formed by dissociative recombination of H_2DO^+/HD_2O^+. Essentially the formation of the water isotopologues proceeds as follows:

$$H_2DO^+ + e^- \Rightarrow HDO + H \quad (7)$$
$$HD_2O^+ + e^- \Rightarrow HDO + D \quad (8)$$
$$CHDCO^+ + e^- \Rightarrow HDO + C_2 \quad (9)$$
$$HD_2DO^+ + e^- \Rightarrow D_2O + H \quad (10)$$
$$D_3O^+ + e^- \Rightarrow D_2O + D \quad (11)$$
$$CD_2CO^+ + e^- \Rightarrow D_2O + C_2 \quad (12)$$

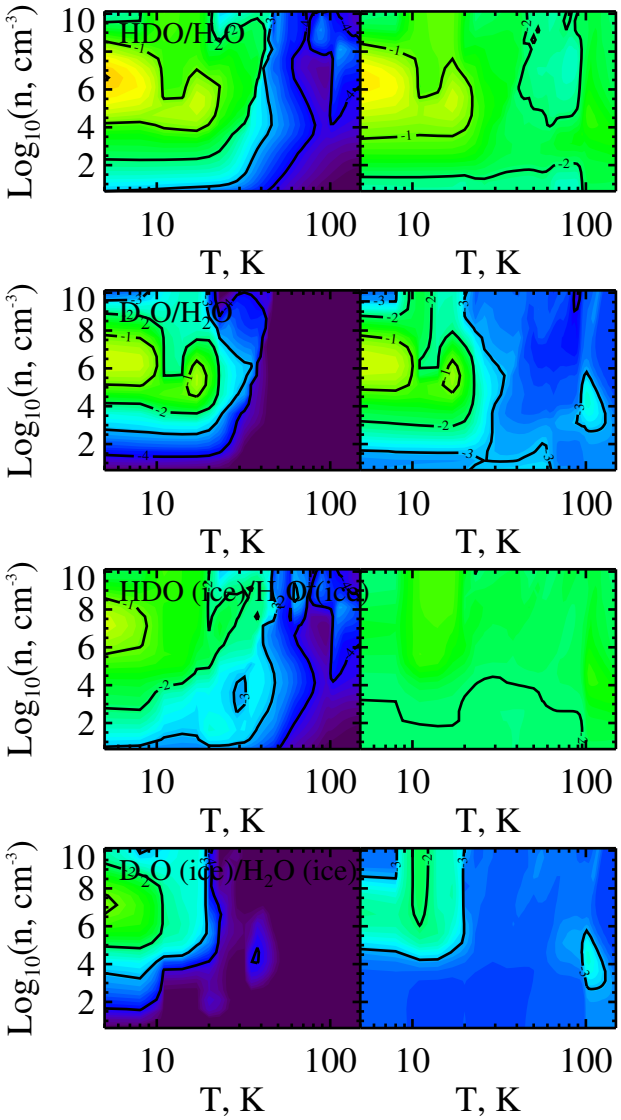

Figure 5. Distribution of the fractionation ratios for the isotopologues of H_2O.

The listed reactions dominate throughout the considered parameter space, but toward higher densities reactions with HCN/HNC also become significant. The main reactants H_2DO^+ and HD_2O^+ are dependent on the isotopologues of H_3^+ through the intermediate formation of HDO^+. Thus, the temperature-dependence becomes somewhat diluted by the intermediate reactions pathways. The decrease in D/H for water occurs at a slightly lower temperature than for H_2D^+, due to the longer, slower evolution of HDO and D_2O. The full list of dominant reaction channels for H_2DO^+ and HD_2O^+ are listed in Table B2. There are two dominant surface reactions, but we note that desorption only plays a small role in increasing the abundance of the H_3O^+ isotopologues, only at higher temperatures does it become significant.

In the "Evolution" model, HDO has an almost constant fractionation ratio over the whole parameter space, both in the gas-phase and on grains. The HDO abundances are quickly accumulated in the previous cold evolutionary phase used as an input for the "Evolution" model. Since the mass difference between HDO and H_2O is only 5%, both these species stick to and desorb from dust grains at similar physical con-

ditions. Consequently, their abundance ratio remains nearly constant at a wide range of T and $n_{\rm H}$, particularly for their ices. While HDO is able to retain a high fractionation ratio ($\gtrsim 10^{-3}$), even at high temperatures in the "Evolution" model, D_2O only show a slightly increased D/H ratio at temperatures < 20 K. It is no surprise that D_2O is harder to produce, as most multi-deuterated species have lower abundances compared to their singly-deuterated analogues.

The main destruction pathways for the water isotopologues are listed in Table B3. Overall, the strongest channel for removing deuterated water is depletion onto grains, which becomes dominant after $\sim 10^4 - 10^5$ years. Reactions with different ions such as HCO^+, H_3^+ and C^+, while individually less important, are able together to make a significant contribution to removing water.

3.2.3. *DCO^+ isotopologues*

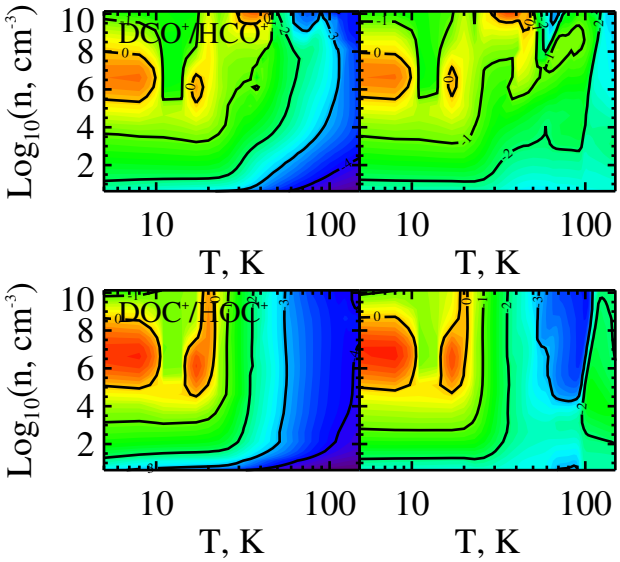

Figure 6. Distribution of fractionation ratios for both gas-phase and iced DOC^+ and DOC^+ in both models.

DCO^+ is an important molecular ion, which is used as a tracer of deuterium fractionation and ionization fraction, and has an isotopomer DOC^+. We distinguish between these two forms in the chemical network, however not in the analysis as we find their evolution similar. The D/H fractionation ratios over the investigated parameter space are plotted in Figure 6, for both DCO^+ and DOC^+. As can be clearly seen, the isotopomers show similar D/H distributions, where the temperature gradient is less smooth for DCO^+ compared to DOC^+. Over the whole parameter space the general fractionation ratio remains at a level of $\sim 10^{-3}$, reaching values as high as > 1 at $T \lesssim 20-30$ K and $n_{\rm H} > 10^5$ cm^{-3}. The same "island" features as in the case of H_3^+ are evident here, which can be attributed to the fact that DCO^+ and DOC^+ are daughter molecules of the H_3^+ isotopologues. This is further strengthened by the similarity in the temperature gradient between these deuterated ions.

In Table B4, the major formation and destruction reactions are listed for the both isotopomers, but essentially the formation proceeds through the following pathways:

$$H_2D^+ + CO \Rightarrow DCO^+ + H_2 \quad (13)$$
$$HD_2^+ + CO \Rightarrow DCO^+ + HD \quad (14)$$
$$D_3 + CO \Rightarrow DCO^+ + D_2 \quad (15)$$
$$N_2D^+ + CO \Rightarrow DCO^+ + N_2 \quad (16)$$

The key formation process is an ion-molecule reaction of CO with different protonated ions. These include the isotopologues of H_3^+, HCO^+ and N_2^+. Another dominant production pathway is a substitute reaction, where HCO^+ react with deuterium, and CH_2D^+ reacting with oxygen. These formation pathways are only dominant in the cold environments where CO is severely depleted from the gas, whereas at higher temperatures the CO production channel dominates. The last pathway is able to change the structure of the isotopomers by reacting with molecular hydrogen, and favoring the formation of more energetically favorable DCO^+ over DOC^+, causing the slight differences for their D/H distributions in the "Primordial" and "Evolution" models.

Key destructive pathways are listed in Table B4, however the most dominant one is the dissociative recombination with electrons, splitting the molecular ions into CO and D. Since CO is the most common reactant to form DCO^+, it will contribute to the reformation of DCO^+. The same is true for the less dominant destruction pathways involving C, HCN/HNC and H, which may be counteracted by the increased CO abundances.

3.2.4. *DCN isotopologues*

Observations of HCN have been extensively used as probes of dense molecular gas and photon-dominated regions (PDRs) (Boger & Sternberg 2005). Both it and its deuterated isotopologue DCN has an isotopomer, DNC, and the formation pathways are similar between the two. Observations of HCN and HNC show an estimated ratio of unity (Herbst et al. 2000), and laboratory studies of DCN and DNC estimate this ratio to be about unity (Hiraoka et al. 2006). Therefore, in the analysis we do not discern between the reaction pathways of the two structural configurations of DCN.

In Figure 7 the fractionation ratios for the gas-phase and solid DCN and DNC are plotted. The corresponding D/H ratios reach levels of $\gtrsim 10\%$ and more, until the temperature barrier of ~ 80 K is reached, at which it drops down to the cosmic level ($\sim 10^{-5}$). Just as for DCO^+, the temperature barrier is not well defined, possibly due to a dependence on the H_3^+ isotopologues diluted by intermediate reactions. There are extended features of high D/H visible at high temperatures ($T \sim 40-50$ K) for the "Evolution" model, most prominently for DCN.

The D/H distribution suggest that the chemical evolution of the HCN/HNC isotopologues is strongly coupled to that of HCO^+ and H_3^+. The key formation pathways are listed in Table B5, but essentially the formation proceeds through the following reaction pathways:

$$H_2D^+ + HCN/HNC \Rightarrow HDCN^+ + H_2 \quad (17)$$
$$HD_2^+ + HCN/HNC \Rightarrow D_2CN^+ + H_2 \quad (18)$$
$$HDCN^+ + e^- \Rightarrow DCN/DNC + H \quad (19)$$
$$D_2CN^+ + e^- \Rightarrow DCN/DNC + D \quad (20)$$
$$HCN/HNC + D \Rightarrow DCN/DNC + H \quad (21)$$

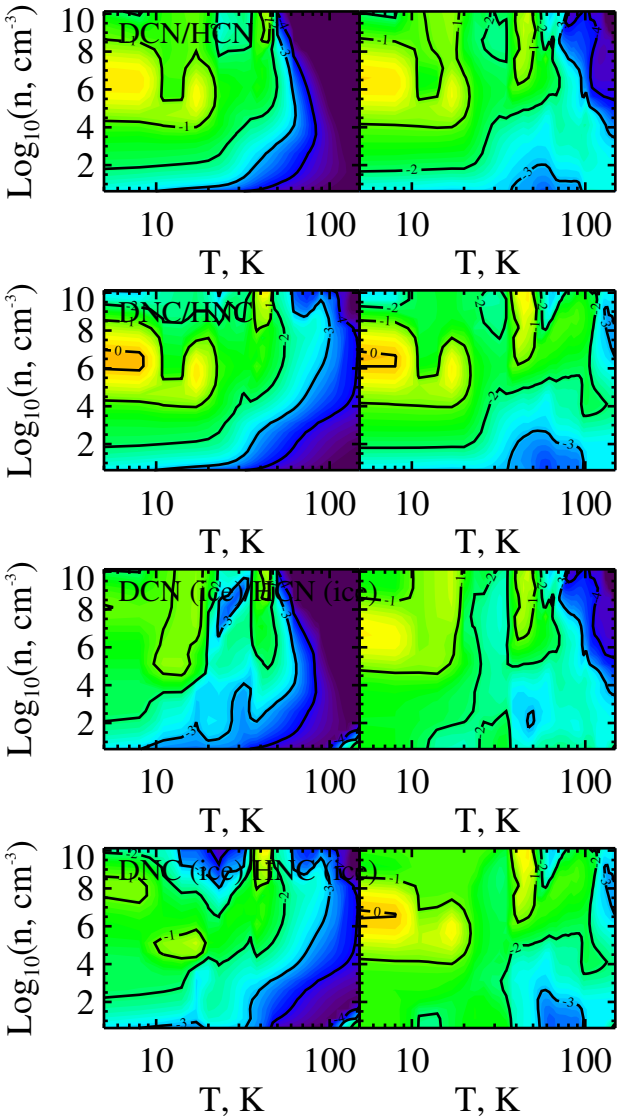

Figure 7. Comparing results between the two models for the DCN/HCN ratio over the investigated parameter space.

Neither of the formation reactions include any of the H_3^+ isotopologues as reactants. Instead, this dependence originates through other reactants such as $HDCN^+$ and D_2CN^+ in reactions 19 and 20, which depend on the H_3^+ isotopologues through reactions 17 and 18. The H_3^+ isotopologues react with HCN/HNC, further increasing the fractionation ratios. DNC/DCN can also form through HNC/HCN reacting with a deuterium atom in reaction 21, but is in general only dominant during the first $10^4 - 10^5$ years of evolution.

The HCN/HNC isotopomers are mainly destroyed by reactions with different ions such as H_3^+, HCO^+ and He^+. Relative to the three main formation pathways however, they are small, and the only effect they have is to slightly slow down the chemical evolution. Freeze-out is instead the main channel for removing DCN and DNC, but it is only dominant at higher densities ($\sim 10^8$ cm^{-3}), while at higher temperature (~ 100 K) it is counteracted by thermal desorption.

3.2.5. *Complex organics: methanol isotopologues*

Complex organics are suggested to be the starting blocks of more advanced molecules essential in the evolution of life, such as amino acids, the structural units for proteins. Many of them are also excellent probes of the surface chemistry in the mid-plane and molecular layer of protoplanetary disks (Semenov 2010). Since they form primarily in cold environments, they are also of interest for investigation in the earlier stages of the interstellar medium.

In Figure 8, the D/H fractionation ratios of the CH_3OH isotopologues are plotted for both models. The D/H distribution is not as smooth as for other species which we have previously discussed, and we see lower fractionation ratios toward higher temperatures. The ratios can reach well above unity for CH_2DOH, especially in "Evolution" model, and orders of magnitude lower for the other two isotopologues. An "island"-like variation of the methanol D/H ratios are also noticeable in Figure 8, especially for CHD_2OH.

Much as for other species, there are significant differences between the two models. The D/H ratio for methanol remain well above the cosmic level in the "Evolution" toward higher temperatures, though in the "Primordial" model this trend is less pronounced. CH_2DOH is able to retain fractionation levels above unity in a substantial region of the parameter space in the both models. In the "Evolution" model all multi-D methanol isotopologues have D/H ratios that are well above the cosmic level, whereas in the "Primordial" model this is true only at $T \lesssim 50$ K.

There is a dependence on the physical properties that affects the methanol production pathways. Initially in the "Primordial" model, up to approximately $10^2 - 10^5$ years (depending on density), reactions 22 - 24 are the primary formation pathways. Later, the other isotopologues become dominant, such as CH_3OHD^+, $CH_3OD_2^+$ and CH_2DOHD^+, also reacting with free electrons. At higher temperatures, desorption becomes significant, eventually reaching an equilibrium between desorption and freeze-out.

$$CH_2DOH_2^+ + e^- \Rightarrow CH_2DOH + H \quad (22)$$
$$CHD_2OH_2^+ + e^- \Rightarrow CHD_2OH + H \quad (23)$$
$$CD_3OH_2^+ + e^- \Rightarrow CD_3OH + H \quad (24)$$

In the "Evolution" model, the formation pathways are the same but less effective. Instead, desorption and freeze-out of pristine methanol dominate. At densities $\gtrsim 10^5$ cm^{-3} freeze-out is the strongest, and at temperatures above ~ 70 K desorption dominates. The CH_3OH isotopologues are only formed in the colder (≤ 50 K) environments, and elsewhere the environment reach a state of equilibrium after ~ 100 years.

Many small destruction pathways are active throughout the evolution, their individual contribution to the net abundance change is, however, less than 10%. The most active reactions are listed in Table B6, showing that there are not many reactions competing in the formation and destruction of the CH_3OH isotopologues. The same reaction pathways are active in the both models, however at somewhat lower rates in the "Evolution" model, where also freeze-out is active as well as some minor desorption channels.

The isotopologues of $CH_3OH_2^+$ are the reactants of the dominant formation pathways, and are formed in a chain of reactions mainly consisting of molecules like CH_n^+ reacting with H_2 or H_2O. The un-deuterated equivalent chain of processes is presented in Eq. 25. We see that there is a chemical link, albeit weak, between the isotopologues of CH_3OH and

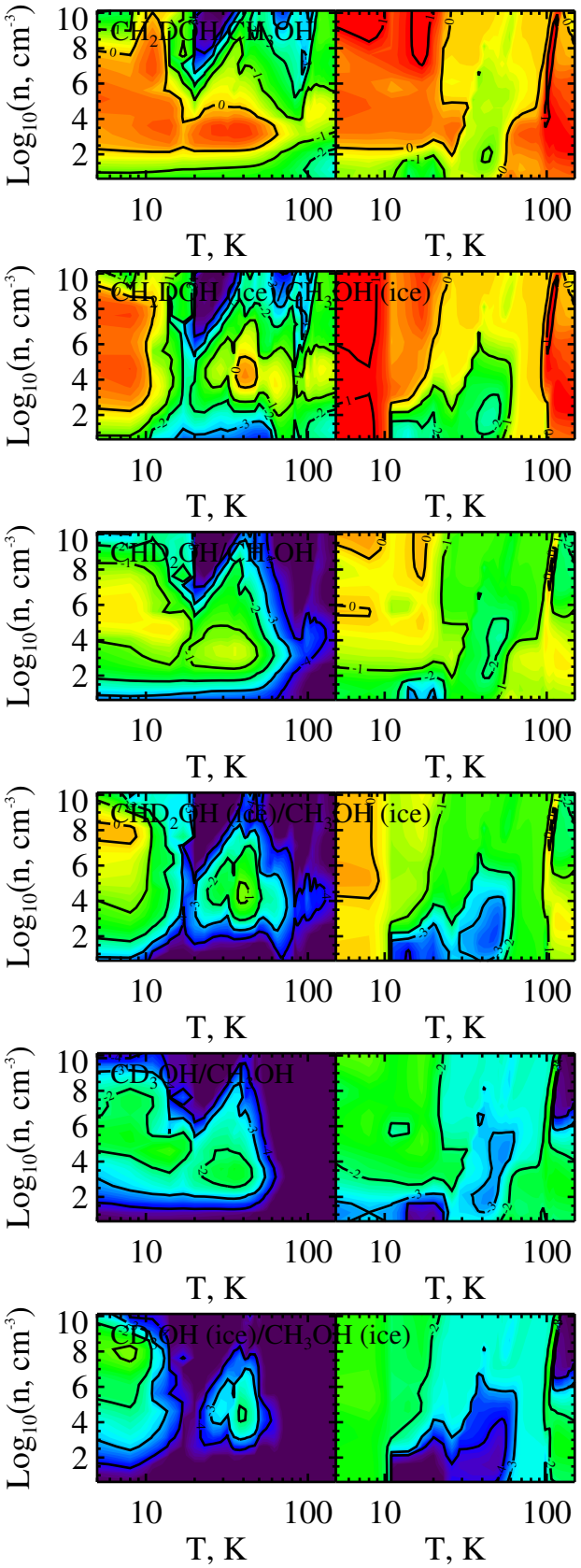

Figure 8. Distribution of fractionation ratios for the isotopologues of CH_3OH, both in gas-phase and on ices.

the H_3^+ isotopologues.

$$\begin{aligned} H_3^+ + C &\Rightarrow CH^+ + H_2 \\ CH^+ + H_2 &\Rightarrow CH_2^+ + H \\ CH_2^+ + H_2 &\Rightarrow CH_3^+ + H \\ CH_3^+ + H_2O &\Rightarrow CH_3OH_2^+ \end{aligned} \quad (25)$$

The lack of smoothness in the plots may stem from the fact that the chemistry of complex organics are not very well-known yet, and involve many surface reaction pathways, part of which is missing in our chemical network (Herbst & van Dishoeck 2009). This could also be the "feature" of the model, where slight delays with the evolution (or evaporation) of D-species compared to lighter H-species can cause strong alterations in respective D/H ratios over a tiny range of temperatures and densities, which show up as local peaks and drops of D/H in the figures.

4. DISCUSSION

4.1. *Observation*

Many deuterated species have been observed in the ISM, protostellar envelopes, and protoplanetary disks in the recent years, and we compare their abundances with predictions of our extended deuterium network. A list of observed deuterated species and their D/H fractions are presented in Table C1, where we also list the corresponding model values and the spatial scale of the observed objects. We have listed the most abundant deuterated species for environments of dark clouds (Table 4), infrared dark clouds (IRDC, Table 5), high-mass protostellar objects (HMPOs, Table 6) and hot cores (Table 7), the full list is available upon request from authors.

The modeled values are chosen in an interval of the considered parameter space that is typical of the observed object. For example, dark clouds are the coldest and less dense environments, whereas hot cores/corinos are the hottest and the densest. Class -I objects (prestellar cores) typically have temperatures 10 K and densities 10^4 cm^{-3}. It is in these objects that the majority of deuterated species have been observed and detected. Class 0 objects (warm protostellar envelopes) have temperatures $> 20-50$ K and higher densities of $\sim 10^4 - 10^6$ cm^{-3}. The Class I objects (hot cores/corinos) have temperatures $\gtrsim 100$ K and densities $\gtrsim 10^6 - 10^8$ cm^{-3}.

As there are substantial error bars associated with the accurate estimation of the physical properties of these objects, e.g. due to uncertainties in dust emissivity, temperature, poorly known dust-to-gas mass ratio, etc., we take our model values from a larger range of temperatures and densities for each class of the environments. Also, many of the published fractionation ratios are based on the measurements made in several sources, and their physical properties can differ significantly, as do the measurements.

The majority of modeled D/H ratios agree well with the observed quantities. Examples are observations in TMC-1 of DCO^+, DCN, HDS, HDCO, NH_2D (van Dishoeck et al. 1995) that fit well within an order of magnitude with our model values. For a number of species, observations have been inconclusive, and only upper limits are available. An example of such is H_2D^+, which has been observed extensively previously, but due to the complexity of observing H_3^+, there is only one available measurement of H_2D^+, merely with upper limits. These isotopologues could possibly become observable with the future ALMA facility.

Table 4
Most abundant deuterated species in cold dark clouds.

Species	Model	Observation
HD	1.45 x 10−5	$10^{-7} - 10^{-5}$ [1, 2, 3, 4]
D	5.04 x 10−6	1.8 - 2.4 x 10^{-5}[5]
D_2	3.02 x 10−7	
HDO (ice)	2.42 x 10−6	
CH_3D (ice)	7.94 x 10−7	
NH_2D (ice)	3.44 x 10−7	
OD	2.34 x 10−7	$<$ 2.5 x 10^{-3} [6]
CH_3D	1.51 x 10−7	
HDO	5.98 x 10−8	0.07 [7]
CH_3D (ice)	4.62 x 10−8	

References. — (1) Lacour et al. (2005); (2) Snow & McCall (2006); (3) Balashev et al. (2010); (4) Bacmann et al. (2010); (5) Rogers et al. (2007); (6) Allen et al. (1974); (7) Parise et al. (2005)

Table 5
Most abundant deuterated species in infrared dark clouds (IRDC).

Species	Model	Observation
D	1.01 x 10−5	1.8 - 2.4 x 10^{-5}[1]
HD	7.38 x 10−6	$10^{-7} - 10^{-5}$ [2,3,4,5]
HDO (ice)	3.68 x 10−6	
D_2	2.24 x 10−6	
CH_3D (ice)	1.06 x 10−6	
NH_2D (ice)	6.38 x 10−7	
D_2O (ice)	3.38 x 10−7	
CH_2D_2(ice)	2.18 x 10−7	
NHD_2(ice)	2.06 x 10−7	
ND_3(ice)	1.18 x 10−7	

References. — (1) Rogers et al. (2007); (2) Lacour et al. (2005); (3) Snow & McCall (2006); (4) Balashev et al. (2010); (5) Bacmann et al. (2010)

Table 6
Most abundant deuterated species in high-mass protostellar objects.

Species	Model	Observation
HD	2.46 x 10−5	
HDO (ice)	2.26 x 10−6	0.001 - 0.01 [1]
D_2	6.98 x 10−7	
CH_3D	6.30 x 10−7	
D	5.28 x 10−7	
NH_2D (ice)	2.52 x 10−7	
D_2O (ice)	6.96 x 10−8	
CH_2D_2	3.78 x 10−8	
HDO_2	1.83 x 10−8	
NHD_2(ice)	1.57 x 10−8	

References. — (1) Teixeira et al. (1999)

For H_2D^+ and the other isotopologues, we believe to have a good understanding of the basic chemistry thanks to extensive laboratory studies. However in recent years further studies of ortho- and para-modes have been conducted as observations have revealed these modes in the interstellar medium. As our model does not include the modes of the H_3^+ isotopologues and other species, we are unable to fully compare our models with observations.

Also for later evolutionary stages of the interstellar medium, in prestellar cores, and hot cores/corinos, we find that the models are in good agreement with observations. A few species stand out however. For D_2CO, HDCO and NHD_2, our models underestimate the observed values. When comparing our results of these species to the models of Roberts & Millar (2000a), we only find a good agreement with NHD_2. We will discuss this discrepancy further in the comparison

Table 7
Most abundant deuterated species in hot cores.

Species	Model	Observation
HD	2.32 x 10–5	
HDO (ice)	3.92 x 10–6	0.001- 0.01 [1]
D_2	1.05 x 10–6	
CH_3D	4.36 x 10–7	
D	1.17 x 10–7	
HDO	1.06 x 10–7	2.94 x 10^{-2} [2]
D_2O (ice)	5.58 x 10–8	
CH_2D_2	2.66 x 10–8	
NH_2D (ice)	9.56 x 10–9	
CHD_3	4.24 x 10–9	

References. — (1) Teixeira et al. (1999); (2) Butner et al. (2007)

with models.

For a large number of essential species, we have not found any published fractionation ratios, and the reason to this may be the same as for H_3^+, namely a symmetric structure, or the signal is too weak to observe, or it has simply not yet been found. We can however expect a boom of new observations to be revealed with ALMA. Overall, our models are able to reproduce the observed fractionation ratios, and we await anxiously new observations from ALMA for new comparisons.

4.2. *Models*

A multitude of models have been used over the years since the first molecule was observed in interstellar space, evolving to implement larger chemical networks, including multi-deuterated species and surface chemistry. Also physical treatments have improved, such as inclusion of vertical and radial mixing, evolution of physical properties and more.

Incorporating a small network consisting of 2445 gas-phase reactions, linked by 225 species, Rodgers & Millar (1996) investigated the chemical evolution of the deuterium chemistry in hot cores, with $T \gtrsim 100$ K and $n_{\rm H} \simeq 10^7$ cm^{-3}. They looked especially at the evolution of an assortment of species; HDCO, CH_3D, NH_2D, HDO, DC_3N, DNC/DCN, DCO^+, C_2D and OD, which we compared to our model for similar temperature and density range.

The same method was incorporated to our chemical network to incorporate deuterated species, however the deuterium chemistry of Rodgers & Millar (1996) incorporated merely 100 deuterated species linked by 1,000 reactions, while our networks include approximately an order of magnitude more. While we incorporated a normal branching ratio where reaction rates were spread evenly among reaction pathways created through the cloning, they implemented statistical branching ratios, meaning that some species may have increased or decreased abundances due to the changed branching ratios. The results of our models agree well within an order of magnitude. This comparison however is limited to a small set of species, and there may very well be discrepancies in the evolution of other species, as our understanding of many species has evolved since the study of Rodgers & Millar (1996) was conducted.

Roberts & Millar (2000b) did a similar study to ours, looking at the chemical evolution over a parameter space in temperature and density, however over a somewhat tighter parameter space with lower resolution. They implemented a pseudo-time-dependent model that incorporated most reactions from the UMIST97 database (Millar et al. 1997), consisting of almost 300 species linked by over 5,000 reactions. They only included simple surface chemistry for the formation of H_2 and HD, while we include a more extensive network of reactions.

We compare the results of our model for a number of species, including DCO^+, HDCO, DCN/DNC and NH_2D, looking not only at fractionation levels but also the distribution of D/H over the parameter space. We first only compare values for a TMC-1 environment after 10^5 years, and summarize values between our models for several essential deuterated species in Table 8. We note that the agreement is good within an order of magnitude for all but one species; NH_2D, where the fractionation ratios between the models diverge by a multiple of ~ 15. It is difficult to determine the source of this discrepancy, but Roberts & Millar (2000b) implemented the UMIST database, while we base our study on the osu.2009 network. Due to significant difference in rates at low temperatures between these chemical network, we believe it to be the cause of this big discrepancy.

Looking instead at the parameter space study, and the general trends for the same species, we find the biggest discrepancy for DCO^+ and DCN/DNC. For other species the models agree well within the ratio intervals of our models, and we see similar dependencies to temperature and density. For DCO^+ there are significant differences between the models. Where our model keeps a steady fractionation ratio up until very high temperatures of ~ 100 K, theirs drop rapidly already at 20 K. The same goes also for DCN/DNC, with similar distributions as to DCO^+. This, as well, may well be caused by the two different networks implemented, as discussed above.

Roberts & Millar (2000b) only considered singly-deuterated species, but in a connected paper Roberts & Millar (2000a) looked also at multi-deuterated species as well as surface chemistry. They only discuss a limited set of species, but for NH_2D and the isotopologues of water, HDO and D_2O, we find a good agreement.

NHD_2 show ratios at or below the cosmic level in Roberts & Millar (2000a), even at the lowest temperatures, while in the same temperature range our model retain levels of $10^{-3} - 10^{-1}$ up to a temperature $\sim$20 K. However, our models agree with observations, e.g. Roueff et al. (2000, 2005). Once again it is difficult to determine the source of this discrepancy, but we believe it to be caused by the different chemical networks implemented as we discussed previously. In the model where surface chemistry is turned off, HDCO also show considerable differences to our model values, which further show how

Table 8
Comparison of fractionation ratios for TMC-1 environment (T = 10 K, $n_H = 10^4$ cm^{-3}) between our model and Roberts & Millar (2000b).

Species	Our model	Roberts & Millar (2000a)
NH_2D	4.0 x 10^{-3}	8.4 x 10^{-2}
HDCO	5.1 x 10^{-2}	4.2 x 10^{-2}
DCN	2.0 x 10^{-2}	0.9 x 10^{-2}
DNC	1.9 x 10^{-2}	1.5 x 10^{-2}
C_2D	1.6 x 10^{-2}	1.1 x 10^{-2}
C_4 D	1.4 x 10^{-3}	0.4 x 10^{-2}
DCO^+	7.4 x 10^{-2}	1.9 x 10^{-2}
N_2D^+	7.6 x 10^{-2}	2.5 x 10^{-2}
C_3HD	7.4 x 10^{-3}	0.6 x 10^{-2}
C_3H_3D	1.0 x 10^{-2}	8.3 x 10^{-2}
DC_3N	1.1 x 10^{-2}	0.7 x 10^{-2}
DC_5 N	2.7 x 10^{-3}	2.3 x 10^{-2}
HDCS	2.4 x 10^{-2}	4.0 x 10^{-2}

important grain surfaces are as catalysts for organic organic molecules.

In the study of Roberts et al. (2004), two chemical networks; Rate99 and osu2003, were implemented and compared as to their effect on the results. They used the model to explain recent observations of the CO depletion in prestellar cores, and its association to D_2CO and HDCO fractionation ratios, and found reasonably good agreement. Between the two chemical networks, the agreement is good, with fractionation ratios for most deuterated species agreeing well within an order of magnitude. The biggest disagreement occur for some of the sulfur-bearing species, where the reaction networks diverge the most.

Comparing fractionation ratios between our models for TMC-1 environments, the majority of species agree well, including H_2D^+, N_2D^+, DCO^+ and HDO. But a number of species also show big discrepancies between our studies, which dominantly include multi-deuterated species such as D_2O, HD_2^+, D_3^+ and NHD_2. As their study is mainly aimed at investigating the effects of implementing the different chemical networks, Roberts et al. (2004) incorporated only a sub-set of the networks where only species with six or fewer carbon atoms in total were added. Because surface chemistry was not included as well, many essential reaction pathways are missing, which may lead to the big disagreement between our models. This show how sensitive the more complex as well as multi-deuterated species are to the networks, and the dependence on large networks.

In a more recent study, Roueff et al. (2007) used steady-state chemical modeling to confirm recent observations of high fractionation ratios of DCN/HCN in dense clumps of the Orion Bar, observed by Leurini et al. (2006). They incorporated the Meudon gas-phase network (Roueff et al. 2005), including 218 species with multi-deuterated isotopologues involving the elements C, N, O and S, connected by more than 3250 reactions, but only for gas-phase chemistry. They focused on studying the physical conditions of warm clumps, and assume them to be homogeneous, with physical parameter ranging in temperature of $10-70$ K and densities $n_H = 10^4 - 10^7$ cm^{-3}. They incorporate two different initial abundance as well, both atomic, where some material frozen onto grains in cold source is assumed to be desorbed into the gas in one, and the second similar to our adopted cosmic abundance.

Among the discussed species in their study, the majority of species agree well with our models. Three species however show greater discrepancies; DCO^+, HDCO and D_2CO. For DCO^+, there are big differences in the fractionation ratios between the two incorporated models by Roueff et al. (2007). The discrepancy are dependent on the initial abundance adopted, and illustrate how species such as DCO^+ are affected by the initial abundances, even to slight changes.

HDCO and D_2CO show similar fractionation ratios in both model, but the discrepancy stems instead from the lack of surface chemistry. In our models, at low temperatures, significant amounts of HDCO and D_2CO are formed on grain surfaces, and desorbed into the gas phase, being the main source of formation for the species later in the evolution.

4.3. *Conclusions*

We have shown how our model simultaneously can explain observed D/H ratios of both cold and hot environments of the interstellar medium, implementing a simple two-staged evolution model and, to our knowledge, the biggest chemical network for deuterium chemistry to date. Our model is not without its drawbacks however, and we discuss these here and the effects that they may infer on our results.

In the past decade there has been a multitude of studies and experiments that investigate the different structural configurations that species may exist in; ortho, para and meta (Crabtree et al. 2011; Vastel et al. 2010; Pagani et al. 2009; Caselli et al. 2008; Vastel et al. 2006a,b). These modes have been found to play a crucial role in the behavior of several species, including H_2, water, and the isotopologues of H_3^+, and if not taken into account, it can have significant effects on the chemical evolution (Flower et al. 2006). Given the complexity and size of the chemical network, we chose not to include the different modes of deuterated and non-deuterated species.

Our simple evolutionary model, where we simulate a TMC-1 environment for 1 Myr and use the final abundances as the initial abundance for the model, is a very simple approach to the evolution of the interstellar medium during the chemical evolution. It is only a 2-staged model, whereas a number of previous studies have incorporated a continuous evolution of the environment during their evolution. The advantage to our approach is that we are able to look at a much wider parameter space with higher resolution, however, the simple approach of evolutionary model will affect the chemistry through the constant change physical parameters. As we have shown in

Section 3, the chemical evolution of a majority of species is dependent on the temperature, while density only has minor effects on a limited number of species. The increase in temperature may affect the evolution of some species by activating new destructive pathways or releasing important reactants into the gas-phase, enhancing other formation pathways.

Less significant effects on the evolution would come from our choice of simulating a set of homogeneous zero-dimensional objects with varying densities and temperatures. For cold, dark clouds this is valid, as they are more or less homogeneous, but for hot cores/corinos this is not a good approximation anymore, as temperatures especially change drastically with distance from the very centers of the objects. But our parameter space study has the advantage that we can show of the chemistry change throughout the object's structure. Would we simulate hot core/corinos specifically, with a physical size and temperature and density gradients, we would need to include other processes such as mixing in our models, which affect the evolution as well.

Our choice of using normal branching ratios, rather than statistical, may cause over- or under-estimations of reaction rates for certain pathways. However, since the reaction rates of many reaction pathways are uncertain, this effect will not be significant, and rates and branching ratios for the most essential species have already been measured in laboratories.

These simplifications in our models affect our results, but comparing our models with observed D/H ratios we find good agreements for many interstellar molecules, including water, methanol, ammonia and many hydrocarbons. We also have very good agreement with previous model studies by (Roueff et al. 2007; Roberts et al. 2004; Roberts & Millar 2000a,b; Rodgers & Millar 1996), where the most essential species agree within an order of magnitude. The biggest discrepancies all through are for the species DCO^+, HDCO and D_2CO, where the latter two have been better understood after the introduction of surface chemistry into chemical models. DCO^+ has been studied extensively both in laboratories and with telescopes, and our model agree well with the observed values.

We also list the most dominating formation and destruction pathways for DCO^+, DCN and isotopologues of water, H_3^+ and CH_3OH, and note that especially surface reactions are in dire need of updated reactions rates, especially for complex organics such as the CH_3OH isotopologues. With Herschel gathering new measurements from observations, and in the advent of the upcoming ALMA and possibly JWST facilities, we have listed predicted relative abundances of the most abundant deuterated species in low- and high-mass star formation environments of the interstellar medium.

The research leading to these results has received funding from the (European Community's) Seventh Framework Programme [FP7/2007-2013] under grant agreement no. 238258.

REFERENCES

Adams, N. G. & Smith, D. 1985, ApJ, 294, L63
Aikawa, Y. & Herbst, E. 1999, ApJ, 526, 314
Aikawa, Y., Ohashi, N., & Herbst, E. 2003, ApJ, 593, 906
Allen, M., Cesarsky, D. A., & Crutcher, R. M. 1974, ApJ, 188, 33
Alonso-Albi, T., Fuente, A., Crimier, N., et al. 2010, A&A, 518, A52+
Anderson, I. M., Caselli, P., Haikala, L. K., & Harju, J. 1999, A&A, 347, 983
André, P., Basu, S., & Inutsuka, S. 2009, The formation and evolution of prestellar cores, ed. Chabrier, G. (Cambridge University Press), 254–+
Bacmann, A. 2003, in SF2A-2003: Semaine de l'Astrophysique Francaise, ed. F. Combes, D. Barret, T. Contini, & L. Pagani, 155–+
Bacmann, A., Caux, E., Hily-Blant, P., et al. 2010, A&A, 521, L42+
Bacmann, A., Lefloch, B., Ceccarelli, C., et al. 2003, ApJ, 585, L55
Bacmann, A., Lefloch, B., Parise, B., Ceccarelli, C., & Steinacker, J. 2007, in Molecules in Space and Laboratory
Balashev, S. A., Ivanchik, A. V., & Varshalovich, D. A. 2010, Astronomy Letters, 36, 761
Bayet, E., Awad, Z., & Viti, S. 2010, ApJ, 725, 214
Bell, M. B., Avery, L. W., Matthews, H. E., et al. 1988, ApJ, 326, 924
Belloche, A., Parise, B., van der Tak, F. F. S., et al. 2006, A&A, 454, L51
Bergman, P., Parise, B., Liseau, R., & Larsson, B. 2011, A&A, 527, A39+
Boger, G. I. & Sternberg, A. 2005, ApJ, 632, 302
Bonev, B. P., Mumma, M. J., Gibb, E. L., et al. 2009, ApJ, 699, 1563
Brown, P. D., Charnley, S. B., & Millar, T. J. 1988, MNRAS, 231, 409
Busquet, G., Palau, A., Estalella, R., et al. 2010, A&A, 517, L6+
Butner, H. M., Charnley, S. B., Ceccarelli, C., et al. 2007, ApJ, 659, L137
Butner, H. M., Lada, E. A., & Loren, R. B. 1995, ApJ, 448, 207
Caselli, P., van der Tak, F. F. S., Ceccarelli, C., & Bacmann, A. 2003, A&A, 403, L37
Caselli, P., Vastel, C., Ceccarelli, C., et al. 2008, A&A, 492, 703
Cazaux, S., Caselli, P., Cobut, V., & Le Bourlot, J. 2008, A&A, 483, 495
Ceccarelli, C. 2002, Planet. Space Sci., 50, 1267
Ceccarelli, C. & Dominik, C. 2005, A&A, 440, 583
Ceccarelli, C., Dominik, C., Caux, E., Lefloch, B., & Caselli, P. 2005, ApJ, 631, L81
Cernicharo, J., Polehampton, E., & Goicoechea, J. R. 2007, ApJ, 657, L21
Cesarsky, D. A., Moffet, A. T., & Pasachoff, J. M. 1973, ApJ, 180, L1+
Chabot, M., Tuna, T., Béroff, K., et al. 2010, A&A, 524, A39+
Charnley, S. B., Tielens, A. G. G. M., & Rodgers, S. D. 1997, ApJ, 482, L203+
Chen, H., Liu, S., Su, Y., & Zhang, Q. 2010, ApJ, 713, L50
Comito, C., Schilke, P., Rolffs, R., et al. 2010, A&A, 521, L38+
Crabtree, K. N., Indriolo, N., Kreckel, H., Tom, B. A., & McCall, B. J. 2011, ApJ, 729, 15
Crapsi, A., Caselli, P., Walmsley, C. M., et al. 2005, ApJ, 619, 379
Crapsi, A., Caselli, P., Walmsley, C. M., et al. 2004, A&A, 420, 957
Croswell, K. & Dalgarno, A. 1985, ApJ, 289, 618
Demyk, K., Bottinelli, S., Caux, E., et al. 2010, A&A, 517, A17+
Emprechtinger, M., Caselli, P., Volgenau, N. H., Stutzki, J., & Wiedner, M. C. 2009, A&A, 493, 89
Emprechtinger, M., Volgenau, N. H., & Wiedner, M. C. 2007, in Molecules in Space and Laboratory
Flower, D. R., Pineau Des Forêts, G., & Walmsley, C. M. 2006, A&A, 449, 621
Fontani, F., Caselli, P., Bourke, T. L., Cesaroni, R., & Brand, J. 2008, A&A, 477, L45
Fontani, F., Caselli, P., Crapsi, A., et al. 2006, A&A, 460, 709
Friesen, R. K., Di Francesco, J., Myers, P. C., et al. 2010, ApJ, 718, 666
Garrod, R. T. & Herbst, E. 2006, A&A, 457, 927
Geiss, J. & Reeves, H. 1981, A&A, 93, 189
Gerin, M., Combes, F., Wlodarczak, G., Encrenaz, P., & Laurent, C. 1992a, A&A, 253, L29
Gerin, M., Combes, F., Wlodarczak, G., et al. 1992b, A&A, 259, L35
Gibb, E. L., Bonev, B. P., Sudholt, E., et al. 2010, in Bulletin of the American Astronomical Society, Vol. 42, AAS/Division for Planetary Sciences Meeting Abstracts #42, 963–+
Giles, K., Adams, N. G., & Smith, D. 1992, The Journal of Physical Chemistry, 96, 7645
Goicoechea, J. R., Pety, J., Gerin, M., Hily-Blant, P., & Le Bourlot, J. 2009, A&A, 498, 771
Goto, M., Usuda, T., Nagata, T., et al. 2008, ApJ, 688, 306
Guilloteau, S., Piétu, V., Dutrey, A., & Guélin, M. 2006, A&A, 448, L5
Harju, J., Haikala, L. K., Lehtinen, K., et al. 2006, A&A, 454, L55
Hatchell, J. 2003, A&A, 403, L25
Hébrard, G. 2006, in Astronomical Society of the Pacific Conference Series, Vol. 348, Astrophysics in the Far Ultraviolet: Five Years of Discovery with FUSE, ed. G. Sonneborn, H. W. Moos, & B.-G. Andersson, 47–+
Heiles, C., McCullough, P. R., & Glassgold, A. E. 1993, ApJS, 89, 271
Herbst, E., Adams, N. G., Smith, D., & Defrees, D. J. 1987, ApJ, 312, 351
Herbst, E., Terzieva, R., & Talbi, D. 2000, MNRAS, 311, 869
Herbst, E. & van Dishoeck, E. F. 2009, ARA&A, 47, 427
Hidaka, H., Watanabe, N., & Kouchi, A. 2006, in American Institute of Physics Conference Series, Vol. 855, Astrochemistry - From Laboratory Studies to Astronomical Observations, ed. R. I. Kaiser, P. Bernath, Y. Osamura, S. Petrie, & A. M. Mebel , 107–112
Hiraoka, K., Mochizuki, N., & Wada, A. 2006, in American Institute of Physics Conference Series, Vol. 855, Astrochemistry - From Laboratory Studies to Astronomical Observations, ed. R. I. Kaiser, P. Bernath, Y. Osamura, S. Petrie, & A. M. Mebel , 86–99
Hirota, T., Ikeda, M., & Yamamoto, S. 2001, ApJ, 547, 814
Hirota, T., Ikeda, M., & Yamamoto, S. 2003, ApJ, 594, 859
Howe, D. A., Millar, T. J., Schilke, P., & Walmsley, C. M. 1994, MNRAS, 267, 59
Jørgensen, J. K. & van Dishoeck, E. F. 2010, ApJ, 725, L172
Kalvans, J. & Shmeld, I. 2011, in IAU Symposium, Vol. 280, IAU Symposium, 212P–+
Katz, N., Furman, I., Biham, O., Pirronello, V., & Vidali, G. 1999, ApJ, 522, 305

Kuan, Y.-J., Chuang, H.-E., Charnley, S., & Huang, H.-C. 2008, in COSPAR, Plenary Meeting, Vol. 37, 37th COSPAR Scientific Assembly, 1640–+
Lacour, S., André, M. K., Sonnentrucker, P., et al. 2005, A&A, 430, 967
Larsson, M., Danared, H., Larson, A., et al. 1997, Phys. Rev. Lett., 79, 395
Launhardt, R., Nutter, D., Ward-Thompson, D., et al. 2010, ApJS, 188, 139
Lee, H.-H., Herbst, E., Pineau des Forets, G., Roueff, E., & Le Bourlot, J. 1996, A&A, 311, 690
Lee, H.-H., Roueff, E., Pineau des Forets, G., et al. 1998, A&A, 334, 1047
Leurini, S., Rolffs, R., Thorwirth, S., et al. 2006, A&A, 454, L47
Linsky, J. L. 2003, Space Sci. Rev., 106, 49
Lis, D. C., Gerin, M., Phillips, T. G., & Motte, F. 2002a, ApJ, 569, 322
Lis, D. C., Roueff, E., Gerin, M., et al. 2002b, ApJ, 571, L55
Liu, F., Parise, B., Kristensen, L., et al. 2011, A&A, 527, A19+
Loinard, L., Castets, A., Ceccarelli, C., et al. 2003, in SFChem 2002: Chemistry as a Diagnostic of Star Formation, ed. C. L. Curry & M. Fich, 351–+
Loinard, L., Castets, A., Ceccarelli, C., et al. 2002, Planet. Space Sci., 50, 1205
MacLeod, J. M., Avery, L. W., & Broten, N. W. 1981, ApJ, 251, L33
Marcelino, N., Cernicharo, J., Roueff, E., Gerin, M., & Mauersberger, R. 2005, ApJ, 620, 308
Margulès, L., Huet, T. R., Demaison, J., et al. 2010, ApJ, 714, 1120
Markwick, A. J., Charnley, S. B., Butner, H. M., & Millar, T. J. 2005, ApJ, 627, L117
Markwick, A. J., Millar, T. J., & Charnley, S. B. 2002, A&A, 381, 560
Miettinen, O., Harju, J., Haikala, L. K., Kainulainen, J., & Johansson, L. E. B. 2009, A&A, 500, 845
Millar, T. J., Bennett, A., & Herbst, E. 1989, ApJ, 340, 906
Millar, T. J., Farquhar, P. R. A., & Willacy, K. 1997, A&AS, 121, 139
Minowa, H., Satake, M., Hirota, T., et al. 1997, ApJ, 491, L63+
Nagaoka, A., Watanabe, N., & Kouchi, A. 2006, in American Institute of Physics Conference Series, Vol. 855, Astrochemistry - From Laboratory Studies to Astronomical Observations, ed. R. I. Kaiser, P. Bernath, Y. Osamura, S. Petrie, & A. M. Mebel , 69–75
Öberg, K. I., Garrod, R. T., van Dishoeck, E. F., & Linnartz, H. 2009a, A&A, 504, 891
Öberg, K. I., Linnartz, H., Visser, R., & van Dishoeck, E. F. 2009b, ApJ, 693, 1209
Öberg, K. I., van Dishoeck, E. F., & Linnartz, H. 2009c, A&A, 496, 281
Osamura, Y., Roberts, H., & Herbst, E. 2004, A&A, 421, 1101
Pagani, L., Vastel, C., Hugo, E., et al. 2009, A&A, 494, 623
Parise, B., Belloche, A., Du, F., Güsten, R., & Menten, K. M. 2011, A&A, 526, A31+
Parise, B., Castets, A., Herbst, E., et al. 2004, A&A, 416, 159
Parise, B., Caux, E., Castets, A., et al. 2005, A&A, 431, 547
Parise, B., Ceccarelli, C., Tielens, A. G. G. M., et al. 2006, A&A, 453, 949
Parise, B., Ceccarelli, C., Tielens, A. G. G. M., et al. 2002, A&A, 393, L49
Parise, B., Leurini, S., Schilke, P., Roueff, E., & Thorwirth, S. 2007, in Molecules in Space and Laboratory
Parise, B., Leurini, S., Schilke, P., et al. 2009, A&A, 508, 737
Parise, B., Simon, T., Caux, E., et al. 2003, A&A, 410, 897
Qi, C., Wilner, D. J., Aikawa, Y., Blake, G. A., & Hogerheijde, M. R. 2008, ApJ, 681, 1396
Roberts, H. 2005, in IAU Symposium, Vol. 231, Astrochemistry: Recent Successes and Current Challenges, ed. D. C. Lis, G. A. Blake, & E. Herbst, 27–36
Roberts, H., Herbst, E., & Millar, T. J. 2003, ApJ, 591, L41
Roberts, H., Herbst, E., & Millar, T. J. 2004, A&A, 424, 905
Roberts, H. & Millar, T. J. 2000a, A&A, 364, 780
Roberts, H. & Millar, T. J. 2000b, A&A, 361, 388
Roberts, H. & Millar, T. J. 2006, Royal Society of London Philosophical Transactions Series A, 364, 3063
Roberts, H. & Millar, T. J. 2007, A&A, 471, 849
Rodgers, S. D. & Millar, T. J. 1996, MNRAS, 280, 1046
Rogers, A. E. E., Dudevoir, K. A., & Bania, T. M. 2007, AJ, 133, 1625
Roueff, E., Lis, D. C., van der Tak, F. F. S., Gerin, M., & Goldsmith, P. F. 2005, A&A, 438, 585
Roueff, E., Parise, B., & Herbst, E. 2007, A&A, 464, 245
Roueff, E., Tiné, S., Coudert, L. H., et al. 2000, A&A, 354, L63
Saito, S., Ozeki, H., Ohishi, M., & Yamamoto, S. 2000, ApJ, 535, 227
Sakai, N., Sakai, T., Hirota, T., & Yamamoto, S. 2009, ApJ, 702, 1025
Schilke, P., Walmsley, C. M., Pineau Des Forets, G., et al. 1992, A&A, 256, 595
Semenov, D. 2010, ArXiv e-prints, 1011.4770
Semenov, D., Hersant, F., Wakelam, V., et al. 2010, A&A, 522, A42+
Shah, R. Y. & Wootten, A. 2001, ApJ, 554, 933
Sidhu, K. S., Miller, S., & Tennyson, J. 1992, A&A, 255, 453
Sipilä, O., Hugo, E., Harju, J., et al. 2010, A&A, 509, A98+
Smith, D., Adams, N. G., & Alge, E. 1982a, J. Chem. Phys., 77, 1261
Smith, D., Adams, N. G., & Alge, E. 1982b, ApJ, 263, 123
Snow, T. P. & McCall, B. J. 2006, ARA&A, 44, 367
Snow, T. P., Ross, T. L., Destree, J. D., et al. 2008, ApJ, 688, 1124
Stancil, P. C., Lepp, S., & Dalgarno, A. 1998, ApJ, 509, 1
Stark, R., van der Tak, F. F. S., & van Dishoeck, E. F. 1999, ApJ, 521, L67
Sundstrom, G., Mowat, J. R., Danared, H., et al. 1994, Science, 263, 785
Teixeira, T. C., Devlin, J. P., Buch, V., & Emerson, J. P. 1999, A&A, 347, L19
Tiné, S., Roueff, E., Falgarone, E., Gerin, M., & Pineau des Forêts, G. 2000, A&A, 356, 1039
Turner, B. E. 1989, ApJ, 347, L39
Turner, B. E. 1990, ApJ, 362, L29
Turner, B. E. 2001, ApJS, 136, 579
van der Tak, F. F. S. 2006, Royal Society of London Philosophical Transactions Series A, 364, 3101
van der Tak, F. F. S., Müller, H. S. P., Harding, M. E., & Gauss, J. 2009, A&A, 507, 347
van der Tak, F. F. S., Schilke, P., Müller, H. S. P., et al. 2002, A&A, 388, L53
van Dishoeck, E. F. 2009, Astrochemistry of Dense Protostellar and Protoplanetary Environments, ed. Thronson, H. A., Stiavelli, M., & Tielens, A., 187–+
van Dishoeck, E. F. & Blake, G. A. 1998, ARA&A, 36, 317
van Dishoeck, E. F., Blake, G. A., Jansen, D. J., & Groesbeck, T. D. 1995, ApJ, 447, 760
van Dishoeck, E. F., Jonkheid, B., & van Hemert, M. C. 2006, Faraday Discussions, 133, 231
Vastel, C. 2007, in SF2A-2007: Proceedings of the Annual meeting of the French Society of Astronomy and Astrophysics, ed. J. Bouvier, A. Chalabaev, & C. Charbonnel, 266–+
Vastel, C., Caselli, P., Ceccarelli, C., et al. 2006a, ApJ, 645, 1198
Vastel, C., Ceccarelli, C., Caux, E., et al. 2010, A&A, 521, L31+
Vastel, C., Phillips, T. G., Caselli, P., Ceccarelli, C., & Pagani, L. 2006b, Royal Society of London Philosophical Transactions Series A, 364, 3081
Vastel, C., Phillips, T. G., Ceccarelli, C., & Pearson, J. 2003, ApJ, 593, L97
Vastel, C., Phillips, T. G., & Yoshida, H. 2004, ApJ, 606, L127
Villanueva, G. L., Mumma, M. J., Bonev, B. P., et al. 2009, ApJ, 690, L5
Wakelam, V., Smith, I. W. M., Herbst, E., et al. 2010, Space Sci. Rev., 156, 13
Walmsley, C. M., Flower, D. R., & Pineau des Forêts, G. 2004, A&A, 418, 1035
Watanabe, N. 2005, in IAU Symposium, Vol. 231, Astrochemistry: Recent Successes and Current Challenges, ed. D. C. Lis, G. A. Blake, & E. Herbst, 415–426
Watson, W. D. 1976, Rev. Mod. Phys., 48, 513
Willacy, K. 2007, ApJ, 660, 441
Willacy, K. & Woods, P. M. 2009, ApJ, 703, 479

APPENDIX

A. UPDATED AND ADDED REACTIONS TO CHEMICAL NETWORK

Table A1 Added and updated non-deuterium reactions.

Reaction			α	β	γ	
CH_2+ H	⇒	CH + H_2	2.20 x 10^{-10}	0.00	0	1
CN + O	⇒	CO + N	2.60 x 10^{-11}	-0.12	0	1
CN + N	⇒	C + N_2	1.00 x 10^{-10}	0.00	0	1
NH + O	⇒	NO + H	6.60 x 10^{-11}	0.00	0	1
C_2+ O	⇒	CO + C	2.00 x 10^{-10}	-0.12	0	1
C_2H + O	⇒	CO + CH	1.00 x 10^{-10}	0.00	0	1
C_3H + O	⇒	C_2H + CO	1.00 x 10^{-10}	0.00	0	1
NO + N	⇒	N_2+ O	4.76 x 10^{-11}	-0.35	0	1
NH_2+ O	⇒	HNO + H	6.39 x 10^{-11}	-0.10	0	1
NH_2+ O	⇒	NH + OH	7.10 x 10^{-12}	0.10	0	1
HNO + O	⇒	NO + OH	3.77 x 10^{-11}	-0.76	0	1
NH_3+ CN	⇒	HCN + NH_2	2.77 x 10^{-11}	-0.85	0	1
C_3N + O	⇒	C_2N + CO	1.00 x 10^{-10}	0.00	0	1
C_2H + N	⇒	CN + CO	1.00 x 10^{-10}	0.00	0	1
C^++ H_2	⇒	CH_2^+	2.00 x 10^{-16}	-1.30	-23	1
$C_2H_2^+$+ H_2	⇒	$C_2H_4^+$	2.90 x 10^{-14}	-1.50	0	1
CH_3^++ H_2	⇒	CH_5^+	3.97 x 10^{-16}	-2.30	22	1
H_3O^++ O	⇒	OH^++ H_2	7.98 x 10^{-10}	-0.156	-1.41	1
H_3O^++ O	⇒	H_2O^++ H	3.42 x 10^{-10}	-0.156	-1.41	1
H_2CO^++ e^+	⇒	HCO + H	1.50 x 10^{-7}	-0.70	0	1
H_2CO^++ e^+	⇒	CO + H + H	2.50 x 10^{-7}	-0.70	0	1
CNC^++ e^+	⇒	CN + C	3.80 x 10^{-7}	-0.60	0	1
$HCNH^+$+ e^+	⇒	HCN + H	9.62 x 10^{-8}	-0.65	0	1
$HCNH^+$+ e^+	⇒	HNC + H	9.62 x 10^{-8}	-0.65	0	1
$HCNH^+$+ e^+	⇒	CN + H + H	9.06 x 10^{-8}	-0.65	0	1
HC_5NH^++ e^+	⇒	C_5N + H_2	8.00 x 10^{-8}	-0.70	0	1
HC_5NH^++ e^+	⇒	HC_5N + H	9.20 x 10^{-7}	-0.70	0	1
HC_5NH^++ e^+	⇒	HCN + HC_4	4.40 x 10^{-7}	-0.70	0	1
HC_5NH^++ e^+	⇒	HNC + HC_4	4.40 x 10^{-7}	-0.70	0	1
HC_5NH^++ e^+	⇒	HC_3N + HC_2	1.20 x 10^{-7}	-0.70	0	1
H_2CO^++ e^+	⇒	CO + H_2	7.50 x 10^{-8}	-0.70	0	1
H_2CO^++ e^+	⇒	CH_2+ O	2.50 x 10^{-8}	-0.70	0	1
CNC^++ e^+	⇒	C_2+ N	2.00 x 10^{-8}	-0.60	0	1
NH_3+ CN	⇒	NH_2CN + H	0.00	0.00	0	1
HNO + O	⇒	NO_2+ H	0.00	0.00	0	1
NH_2+ O	⇒	NO + H_2	0.00	0.00	0	1
O + NH	⇒	OH + N	0.00	0.00	0	1
C_2H + CRPHOT	⇒	C_2+ H	4.05 x 10^3	0.00	0	2
C_3+ CRPHOT	⇒	C_3+ H	3.25 x 10^3	0.00	0	2
C_4 + CRPHOT	⇒	C_3+ C	7.70 x 10^2	0.00	0	2
C_3H_2+ CRPHOT	⇒	C_3H + H	2.30 x 10^3	0.00	0	2
C_4H + CRPHOT	⇒	C_4 + H	2.90 x 10^3	0.00	0	2
C_5 + CRPHOT	⇒	C_4 + C	1.30 x 10^2	0.00	0	2
C_6 + CRPHOT	⇒	C_5 + C	9.00 x 10^1	0.00	0	2
C_7 + CRPHOT	⇒	C_6 + C	1.00 x 10^1	0.00	0	2
C_8 + CRPHOT	⇒	C_7 + C	3.00 x 10^1	0.00	0	2
C_3H^++ e^+	⇒	C_3+ H	1.95 x 10^{-7}	-0.50	0	2
C_3H^++ e^+	⇒	C_2H + C	9.90 x 10^{-8}	-0.50	0	2
$C_3H_2^+$+ e^+	⇒	C_3H + H	1.66 x 10^{-7}	-0.50	0	2
$C_3H_2^+$+ e^+	⇒	C_3+ H_2	8.28 x 10^{-8}	-0.50	0	2
$C_3H_2^+$+ e^+	⇒	C_2H_2+ C	8.64 x 10^{-8}	-0.50	0	2
$C_3H_2^+$+ e^+	⇒	C_2+ CH_2	1.44 x 10^{-8}	-0.50	0	2
C_4H^++ e^+	⇒	C_4 + H	1.74 x 10^{-7}	-0.50	0	2
C_4H^++ e^+	⇒	C_3H + C	7.80 x 10^{-8}	-0.50	0	2
C_4H^++ e^+	⇒	C_2H + C_2	4.80 x 10^{-8}	-0.50	0	2
C_5^++ e^+	⇒	C_4 + C	3.90 x 10^{-8}	-0.50	0	2
C_5^++ e^+	⇒	C_3+ C_2	2.61 x 10^{-7}	-0.50	0	2
C_6^++ e^+	⇒	C_5 + C	1.80 x 10^{-7}	-0.30	0	2
C_6^++ e^+	⇒	C_4 + C_2	2.20 x 10^{-7}	-0.30	0	2
C_7^++ e^+	⇒	C_6 + C	2.30 x 10^{-8}	-0.30	0	2
C_7^++ e^+	⇒	C_5 + C_2	4.37 x 10^{-7}	-0.30	0	2
C_7^++ e^+	⇒	C_4 + C_3	1.84 x 10^{-6}	-0.50	0	2
C_8^++ e^+	⇒	C_7 + C	6.00 x 10^{-8}	-0.30	0	2

Reaction			α	β	γ	
$C_8^+ + e^+$	$\Rightarrow$	$C_6 + C_2$	2.00×10^{-8}	-0.30	0	2
$C_9^+ + e^+$	$\Rightarrow$	$C_7 + C_2$	1.20×10^{-7}	-0.30	0	2
$C_{10}^+ + e^+$	$\Rightarrow$	$C_9 + C$	2.00×10^{-8}	-0.30	0	2
$C_{10}^+ + e^+$	$\Rightarrow$	$C_8 + C_2$	2.00×10^{-8}	-0.30	0	2
C_2H + PHOTON	$\Rightarrow$	$C_2 + H$	8.10×10^{-10}	0.00	0	2
C_3H + PHOTON	$\Rightarrow$	$C_3 + H$	6.50×10^{-10}	0.00	0	2
C_4 + PHOTON	$\Rightarrow$	$C_3 + H$	3.08×10^{-10}	0.00	0	2
C_4 + PHOTON	$\Rightarrow$	$C_2 + C_2$	9.02×10^{-11}	0.00	0	2
C_3H_2 + PHOTON	$\Rightarrow$	$C_3H + H$	1.33×10^{-9}	0.00	0	2
C_3H_2 + PHOTON	$\Rightarrow$	$C_3 + H_2$	6.67×10^{-10}	0.00	0	2
C_4H + PHOTON	$\Rightarrow$	$C_4 + H$	1.16×10^{-9}	0.00	0	2
C_4H + PHOTON	$\Rightarrow$	$C_2H + C_2$	3.20×10^{-9}	0.00	0	2
C_5 + PHOTON	$\Rightarrow$	$C_3 + C_2$	8.70×10^{-12}	0.00	0	2
C_6 + PHOTON	$\Rightarrow$	$C_5 + C$	9.00×10^{-11}	0.00	0	2
C_7 + PHOTON	$\Rightarrow$	$C_6 + C$	1.00×10^{-11}	0.00	0	2
C_8 + PHOTON	$\Rightarrow$	$C_7 + C$	3.00×10^{-11}	0.00	0	2
C_2H + CRPHOT	$\Rightarrow$	$C + CH$	9.50×10^{2}	0.00	0	2
C_3H + CRPHOT	$\Rightarrow$	$C_2H + C$	1.65×10^{3}	0.00	0	2
C_3H + CRPHOT	$\Rightarrow$	$C_2 + CH$	1.00×10^{2}	0.00	0	2
C_4 + CRPHOT	$\Rightarrow$	$C_2 + C_2$	2.30×10^{2}	0.00	0	2
C_3H_2 + CRPHOT	$\Rightarrow$	$C_3 + H_2$	1.20×10^{2}	0.00	0	2
C_3H_2 + CRPHOT	$\Rightarrow$	$C_2H_2 + H$	1.15×10^{3}	0.00	0	2
C_3H_2 + CRPHOT	$\Rightarrow$	$C_2H + CH$	2.00×10^{2}	0.00	0	2
C_3H_2 + CRPHOT	$\Rightarrow$	$C_2 + CH_2$	1.50×10^{2}	0.00	0	2
C_4H + CRPHOT	$\Rightarrow$	$C_3H + C$	1.30×10^{3}	0.00	0	2
C_4H + CRPHOT	$\Rightarrow$	$C_2H + C_2$	8.00×10^{2}	0.00	0	2
C_5 + CRPHOT	$\Rightarrow$	$C_2 + C_2$	8.70×10^{2}	0.00	0	2
C_6 + CRPHOT	$\Rightarrow$	$C_4 + C_2$	1.10×10^{2}	0.00	0	2
C_6 + CRPHOT	$\Rightarrow$	$C_3 + C_3$	8.00×10^{2}	0.00	0	2
C_7 + CRPHOT	$\Rightarrow$	$C_5 + C_2$	1.90×10^{2}	0.00	0	2
C_7 + CRPHOT	$\Rightarrow$	$C_4 + C_3$	8.00×10^{2}	0.00	0	2
C_8 + CRPHOT	$\Rightarrow$	$C_6 + C_2$	1.00×10^{1}	0.00	0	2
C_8 + CRPHOT	$\Rightarrow$	$C_5 + C_3$	9.00×10^{1}	0.00	0	2
C_8 + CRPHOT	$\Rightarrow$	$C_4 + C_4$	6.00×10^{1}	0.00	0	2
C_9 + CRPHOT	$\Rightarrow$	$C_7 + C_2$	6.00×10^{1}	0.00	0	2
C_9 + CRPHOT	$\Rightarrow$	$C_6 + C_3$	6.60×10^{2}	0.00	0	2
C_9 + CRPHOT	$\Rightarrow$	$C_5 + C_4$	2.80×10^{2}	0.00	0	2
$C_3H^+ + e^+$	$\Rightarrow$	$C_2 + CH$	6.00×10^{-9}	-0.50	0	2
$C_3H_2^+ + e^+$	$\Rightarrow$	$C_2H + CH$	1.44×10^{-8}	-0.50	0	2
$C_6^+ + e^+$	$\Rightarrow$	$C_3 + C_3$	1.60×10^{-6}	-0.30	0	2
$C_8^+ + e^+$	$\Rightarrow$	$C_5 + C_3$	1.80×10^{-6}	-0.30	0	2
$C_8^+ + e^+$	$\Rightarrow$	$C_4 + C_4$	1.20×10^{-7}	-0.30	0	2
$C_9^+ + e^+$	$\Rightarrow$	$C_6 + C_3$	1.32×10^{6}	-0.30	0	2
$C_9^+ + e^+$	$\Rightarrow$	$C_5 + C_4$	5.60×10^{-7}	-0.30	0	2
$C_{10}^+ + e^+$	$\Rightarrow$	$C_7 + C_3$	1.40×10^{-6}	-0.30	0	2
$C_{10}^+ + e^+$	$\Rightarrow$	$C_6 + C_4$	6.00×10^{-8}	-0.30	0	2
$C_{10}^+ + e^+$	$\Rightarrow$	$C_5 + C_5$	5.00×10^{-7}	-0.30	0	2
C_2H + PHOTON	$\Rightarrow$	$CH + C$	1.90×10^{-10}	0.00	0	2
C_3H + PHOTON	$\Rightarrow$	$C_2H + C$	3.30×10^{-10}	0.00	0	2
C_3H + PHOTON	$\Rightarrow$	$C_2 + CH$	2.00×10^{-11}	0.00	0	2
C_3H_2 + PHOTON	$\Rightarrow$	$C_2H_2 + C$	1.33×10^{-9}	0.00	0	2
C_3H_2 + PHOTON	$\Rightarrow$	$C_2H + CH$	1.16×10^{-10}	0.00	0	2
C_3H_2 + PHOTON	$\Rightarrow$	$CH_2 + C_2$	1.16×10^{-10}	0.00	0	2
C_4H + PHOTON	$\Rightarrow$	$C_3H + C$	5.20×10^{-10}	0.00	0	2
C_5 + PHOTON	$\Rightarrow$	$C_4 + C$	1.30×10^{-12}	0.00	0	2
C_6 + PHOTON	$\Rightarrow$	$C_4 + C$	1.10×10^{-10}	0.00	0	2
C_6 + PHOTON	$\Rightarrow$	$C_3 + C_3$	8.00×10^{-10}	0.00	0	2
C_7 + PHOTON	$\Rightarrow$	$C_5 + C_2$	1.90×10^{-10}	0.00	0	2
C_7 + PHOTON	$\Rightarrow$	$C_4 + C_3$	8.00×10^{-10}	0.00	0	2
C_8 + PHOTON	$\Rightarrow$	$C_6 + C_2$	1.00×10^{-11}	0.00	0	2
C_8 + PHOTON	$\Rightarrow$	$C_5 + C_3$	9.00×10^{-10}	0.00	0	2
C_8 + PHOTON	$\Rightarrow$	$C_4 + C_4$	6.00×10^{-11}	0.00	0	2
C_9 + PHOTON	$\Rightarrow$	$C_7 + C_2$	6.00×10^{-11}	0.00	0	2
C_9 + PHOTON	$\Rightarrow$	$C_6 + C_3$	6.60×10^{-10}	0.00	0	2
C_9 + PHOTON	$\Rightarrow$	$C_5 + C_4$	2.80×10^{-10}	0.00	0	2
C_{10} + PHOTON	$\Rightarrow$	$C_9 + C$	1.14×10^{-11}	0.00	0	2
C_{10} + PHOTON	$\Rightarrow$	$C_8 + C_2$	1.14×10^{-11}	0.00	0	2
C_{10} + PHOTON	$\Rightarrow$	$C_7 + C_3$	7.98×10^{-10}	0.00	0	2
C_{10} + PHOTON	$\Rightarrow$	$C_6 + C_4$	3.42×10^{-11}	0.00	0	2
C_{10} + PHOTON	$\Rightarrow$	$C_5 + C_5$	2.50×10^{-10}	0.00	0	2

Reaction			α	β	γ	
C_9 + PHOTON	$\Rightarrow$	C_8 + C	0	0.00	0	2
C_9^+ + e^+	$\Rightarrow$	C_8 + C	0	0.00	0	2
C_9 + CRPHOT	$\Rightarrow$	C_8 + C	0	0.00	0	2
C_4H^+ + e^+	$\Rightarrow$	C_3 + CH	0	0.00	0	2
H_3^+ + e^+	$\Rightarrow$	H_2 + H	1.36×10^{-8}	-0.50	0	3
H_3^+ + e^+	$\Rightarrow$	H + H + H	5.44×10^{-8}	-0.50	0	3
$C_2H_2^+$ + H_2	$\Rightarrow$	$C_2H_4^+$	2.30×10^{-14}	-1.50	0	3
CH_3^+ + H_2O	$\Rightarrow$	$CH_3OH_2^+$	5.50×10^{-12}	-1.70	0	3
CN + N	$\Rightarrow$	N_2 + C	1.00×10^{-10}	0.18	0	4
CH_4 + CH	$\Rightarrow$	C_2H_4 + H	1.06×10^{-10}	-1.04	0	4
H_2 + CH	$\Rightarrow$	CH_2 + H	1.20×10^{-9}	0.00	0	4
CH_3^+ + H_2	$\Rightarrow$	CH_5^+	3.78×10^{-16}	-2.30	0	4
$C_5H_2N^+$ + e^+	$\Rightarrow$	HCN + C_4H	8.00×10^{-8}	-0.70	0	4
$C_5N_2N^+$ + e^+	$\Rightarrow$	HC_5N + H	9.20×10^{-7}	-0.70	0	4
$C_5H_2N^+$ + e^+	$\Rightarrow$	HCN + C_4H	4.40×10^{-7}	-0.70	0	4
$C_5H_2N^+$ + e^+	$\Rightarrow$	HNC + C_4H	4.40×10^{-7}	-0.70	0	4
$C_5C_2N^+$ + e^+	$\Rightarrow$	HC_3N + C_2H	1.20×10^{-7}	-0.70	0	4

References. — (1) Wakelam et al. (2010); (2) Chabot et al. (2010); (3) Roberts et al. (2004); (4) KIDA database

Table A2 Added and updated deuterium reactions.

Reaction			α	β	γ	Refs.
$H_3^+ + HD$	$\Rightarrow$	$H_2D^+ + H_2$	1.70 x 10^{-9}	0.00	0.00	1
$H_2D^+ + H_2$	$\Rightarrow$	$H_3^+ + HD$	1.70 x 10^{-9}	0.00	220	1
$H_3^+ + D_2$	$\Rightarrow$	$H_2D^+ + HD$	3.50 x 10^{-10}	0.00	0	2
$H_2D^+ + HD$	$\Rightarrow$	$H_3^+ + D_2$	3.50 x 10^{-10}	0.00	63	2
$H_3^+ + D_2$	$\Rightarrow$	$HD_2^+ + H_2$	1.10 x 10^{-9}	0.00	0	2
$HD_2^+ + H_2$	$\Rightarrow$	$H_3^+ + D_2$	1.10 x 10^{-9}	0.00	251	2
$H_2D^+ + HD$	$\Rightarrow$	$HD_2^+ + H_2$	8.10 x 10^{-10}	0.00	0	2
$HD_2^+ + H_2$	$\Rightarrow$	$H_2D^+ + HD$	8.10 x 10^{-10}	0.00	187	2
$H_2D^+ + D_2$	$\Rightarrow$	$HD_2^+ + HD$	7.00 x 10^{-10}	0.00	0	2
$HD_2^+ + HD$	$\Rightarrow$	$H_2D^+ + D_2$	7.00 x 10^{-10}	0.00	107	2
$H_2D^+ + D_2$	$\Rightarrow$	$D_3^+ + H_2$	7.00 x 10^{-10}	0.00	0	2
$D_3^+ + H_2$	$\Rightarrow$	$H_2D^+ + D_2$	7.00 x 10^{-10}	0.00	341	2
$HD_2^+ + HD$	$\Rightarrow$	$D_3^+ + H_2$	6.40 x 10^{-10}	0.00	0	2
$D_3^+ + H_2$	$\Rightarrow$	$HD_2^+ + HD$	6.40 x 10^{-10}	0.00	234	2
$HD_2^+ + D_2$	$\Rightarrow$	$D_3^+ + HD$	8.70 x 10^{-10}	0.00	0	2
$D_3^+ + HD$	$\Rightarrow$	$HD_2^+ + D_2$	8.70 x 10^{-10}	0.00	159	2
$CH_2D^+ + HD$	$\Rightarrow$	$CHD_2^+ + H_2$	1.60 x 10^{-9}	0.00	0	3
$CHD_2^+ + H_2$	$\Rightarrow$	$CH_2D^+ + HD$	1.60 x 10^{-9}	0.00	370	3
$CHD_2^+ + HD$	$\Rightarrow$	$CD_3^+ + H_2$	1.50 x 10^{-9}	0.00	0	3
$CD_3^+ + H_2$	$\Rightarrow$	$CHD_2^+ + HD$	1.50 x 10^{-9}	0.00	370	3
$CH_3^+ + D_2$	$\Rightarrow$	$CH_2D^+ + HD$	4.40 x 10^{-10}	0.00	0	3
$CH_2D^+ + HD$	$\Rightarrow$	$CH_3^+ + D_2$	4.40 x 10^{-10}	0.00	400	3
$CH_3^+ + D_2$	$\Rightarrow$	$CHD_2^+ + H_2$	6.60 x 10^{-10}	0.00	0	3
$CHD_2^+ + H_2$	$\Rightarrow$	$CH_3^+ + D_2$	6.60 x 10^{-10}	0.00	400	3
$CH_2D^+ + D_2$	$\Rightarrow$	$CHD_2^+ + HD$	1.20 x 10^{-9}	0.00	0	3
$CHD_2^+ + HD$	$\Rightarrow$	$CH_2D^+ + D_2$	1.20 x 10^{-9}	0.00	400	3
$H_2D^+ + D$	$\Rightarrow$	$HD_2^+ + H$	2.00 x 10^{-9}	0.00	0	4
$HD_2^+ + H$	$\Rightarrow$	$H_2D^+ + D$	2.00 x 10^{-9}	0.00	550	4
$HD_2^+ + D$	$\Rightarrow$	$D_3^+ + H$	2.00 x 10^{-9}	0.00	0	4
$D_3^+ + H$	$\Rightarrow$	$HD_2^+ + D$	2.00 x 10^{-9}	0.00	655	4
$CH_3^+ + HD$	$\Rightarrow$	$CH_2D^+ + H_2$	1.30 x 10^{-9}	0.00	0	3
$CH_2D^+ + H_2$	$\Rightarrow$	$CH_3^+ + HD$	8.70 x 10^{-10}	0.00	370	3
$D^+ + H_2$	$\Rightarrow$	$H^+ + HD$	2.10 x 10^{-9}	0.00	0	3
$H^+ + HD$	$\Rightarrow$	$D^+ + H_2$	1.00 x 10^{-9}	0.00	464	3
$C_2H_2^+ + HD$	$\Rightarrow$	$C_2HD^+ + H_2$	1.00 x 10^{-9}	0.00	0	5
$C_2HD^+ + H^+$	$\Rightarrow$	$C_2H_2^+ + HD$	2.50 x 10^{-9}	0.00	550	5
$D^+ + H$	$\Rightarrow$	$H^+ + D$	1.00 x 10^{-9}	0.00	0	6
$H^+ + D$	$\Rightarrow$	$D^+ + H$	1.00 x 10^{-9}	0.00	41	6
$H_3^+ + D$	$\Rightarrow$	$H_2D^+ + H$	1.00 x 10^{-9}	0.00	0	7*
$H_2 + H$	$\Rightarrow$	$H_3^+ + D$	1.00 x 10^{-9}	0.00	632	7
$HCO^+ + D$	$\Rightarrow$	$DCO^+ + H$	1.00 x 10^{-9}	0.00	0	7
$DCO^+ + H$	$\Rightarrow$	$HCO^+ + D$	2.20 x 10^{-9}	0.00	796	7
$N_2H^+ + D$	$\Rightarrow$	$N_2D^+ + H$	1.00 x 10^{-9}	0.00	0	7
$N_2D^+ + H$	$\Rightarrow$	$N_2H^+ + D$	2.20 x 10^{-9}	0.00	550	7
OH + D	$\Rightarrow$	OD + H	1.30 x 10^{-10}	0.50	0	8
OD + H	$\Rightarrow$	OH + D	1.30 x 10^{-10}	0.50	810	8
C_2H + D	$\Rightarrow$	C_2D + H	5.00 x 10^{-11}	0.50	250	9
C_2D + H	$\Rightarrow$	C_2H + D	5.00 x 10^{-11}	0.50	832	9
HCN + D	$\Rightarrow$	DCN + H	1.00 x 10^{-10}	0.50	500	9*
DCN + H	$\Rightarrow$	HCN + D	1.00 x 10^{-10}	0.50	500	9*
$H_2D^+ + e^-$	$\Rightarrow$	HD + H	1.20 x 10^{-8}	-0.50	0	10
$H_2D^+ + e^-$	$\Rightarrow$	H_2 + D	4.20 x 10^{-9}	-0.50	0	10
$H_2D^+ + e^-$	$\Rightarrow$	D + H + H	4.38 x 10^{-8}	-0.50	0	10
$HD_2^+ + e^-$	$\Rightarrow$	HD + D	4.20 x 10^{-9}	-0.50	0	11
$HD_2^+ + e^-$	$\Rightarrow$	D_2 + H	1.20 x 10^{-8}	-0.50	0	11
$HD_2^+ + e^-$	$\Rightarrow$	D + D + H	4.38 x 10^{-8}	-0.50	0	11
$D_3^+ + e^-$	$\Rightarrow$	D_2 + D	5.40 x 10^{-9}	-0.50	0	12
$D_3^+ + e^-$	$\Rightarrow$	D + D + D	2.16 x 10^{-8}	-0.50	0	12
$CH_3^+ + D_2$	$\Rightarrow$	$CH_3D_2^+$	3.50 x 10^{-14}	-1.00	0	12
$CH_2D^+ + H_2$	$\Rightarrow$	CH_4D^+	2.00 x 10^{-14}	-1.00	0	12
$CH_2D^+ + HD$	$\Rightarrow$	$CH_3D_2^+$	3.50 x 10^{-14}	-1.00	0	12
$CHD_2^+ + H_2$	$\Rightarrow$	$CH_3D_2^+$	3.50 x 10^{-14}	-1.00	0	12
$CD_3^+ + H_2$	$\Rightarrow$	$CH_2D_3^+$	6.30 x 10^{-14}	-1.00	0	12
$C_2H_2^+ + H_2$	$\Rightarrow$	$C_2H_3D^+$	3.39 x 10^{-14}	-1.50	0	12
$CH_3^+ + HDO$	$\Rightarrow$	CH_3OHD^+	1.10 x 10^{-11}	-1.70	0	12
$CH_3^+ + D_2O$	$\Rightarrow$	$CH_3OD_2^+$	1.65 x 10^{-11}	-1.70	0	12
$CH_2D^+ + H_2O$	$\Rightarrow$	$CH_2DOH_2^+$	1.10 x 10^{-11}	-1.70	0	12
$CH_2D^+ + H_2O$	$\Rightarrow$	$CH_2DOH_2^+$	1.65 x 10^{-11}	-1.70	0	12
$CH_2D^+ + D_2O$	$\Rightarrow$	$CH_2DOD_2^+$	2.20 x 10^{-11}	-1.70	0	12

Reaction			α	β	γ	Refs.
$CHD_2^+ + H_2O$	$\Rightarrow$	$CHD_2OH_2^+$	1.65 x 10^{-11}	-1.70	0	12
$CHD_2^+ + HDO$	$\Rightarrow$	CHD_2OHD^+	2.20 x 10^{-11}	-1.70	0	12
$CHD_2^+ + D_2O$	$\Rightarrow$	$CHD_2OD_2^+$	2.75 x 10^{-11}	-1.70	0	12
$CD_3^+ + H_2O$	$\Rightarrow$	$CD_3OH_2^+$	2.20 x 10^{-11}	-1.70	0	12
$CD_3^+ + HDO$	$\Rightarrow$	CD_3OHD^+	2.75 x 10^{-11}	-1.70	0	12
$CD_3^+ + D_2$	$\Rightarrow$	$CD_3OD_2^+$	2.75 x 10^{-11}	-1.70	0	12
$CH_3^+ + HD$	$\Rightarrow$	CH_4D^+	0.00	0.00	0	11
$CH_2D^+ + D_2$	$\Rightarrow$	$CH_2D_3^+$	0.00	0.00	0	11
$CHD_2^+ + HD$	$\Rightarrow$	$CH_2D_3^+$	0.00	0.00	0	11
$C_2H_2^+ + H_2$	$\Rightarrow$	$C_2H_3^+$	0.00	0.00	0	11

References. — (1) Ceccarelli & Dominik (2005); (2) Giles et al. (1992); (3) Smith et al. (1982a,b); (4) Walmsley et al. (2004); (5) Herbst et al. (1987); (6) Watson (1976); (7) Adams & Smith (1985); (8) Croswell & Dalgarno (1985); (9) Schilke et al. (1992); (10) Sundstrom et al. (1994); (11) Roberts et al. (2004); (12) Larsson et al. (1997)

* Estimate

Table B1
Most essential formation and destruction pathways for deuterated H_3^+; H_2D^+, HD_2^+ and H_3^+.

Reaction			Rates	Accuracy
$H_3^+ + HD$	$\Rightarrow$	$H_2D^+ + H_2$	1.70E-09 0.00E+00 0.00E+00	(C)(1)
$H_3^+ + D$	$\Rightarrow$	$H_2D^+ + H$	1.00E-09 0.00E+00 0.00E+00	(C)(2)
$H_2D^+ + HD$	$\Rightarrow$	$HD_2^+ + H_2$	8.10E-10 0.00E+00 0.00E+00	$\pm$15% (L) (3)
$H_2D^+ + D$	$\Rightarrow$	$HD_2^+ + H$	2.00E-09 0.00E+00 0.00E+00	(4)
$H_3^+ + D_2$	$\Rightarrow$	$HD_2^+ + H_2$	1.10E-09 0.00E+00 0.00E+00	$\pm$15% (L) (3)
$HD_2^+ + HD$	$\Rightarrow$	$D_3^+ + H_2$	6.40E-10 0.00E+00 0.00E+00	$\pm$15% (L) (3)
$HD_2^+ + D$	$\Rightarrow$	$D_3^+ + H$	2.00E-09 0.00E+00 0.00E+00	(4)
$H_2D^+ + D_2$	$\Rightarrow$	$D_3^+ + H_2$	7.00E-10 0.00E+00 0.00E+00	$\pm$15% (L) (3)
$H_2D^+ + CO$	$\Rightarrow$	$DCO^+ + H_2$	3.22E-10 0.00E+00 0.00E+00	< 25% (M)(5)
$H_2D^+ + CO$	$\Rightarrow$	$HCO^+ + HD$	3.22E-10 0.00E+00 0.00E+00	< 25% (M)(5)
$HD_2^+ + CO$	$\Rightarrow$	$DCO^+ + HD$	3.22E-10 0.00E+00 0.00E+00	< 25% (M)(5)
$HD_2^+ + CO$	$\Rightarrow$	$HCO^+ + H_2$	3.22E-10 0.00E+00 0.00E+00	< 25% (M)(5)
$D_3^+ + CO$	$\Rightarrow$	$DCO^+ + D_2$	3.22E-10 0.00E+00 0.00E+00	< 25% (M)(5)
$D_3^+ + e^-$	$\Rightarrow$	D + D + D	2.16E-08 -0.50E+00 0.00E+00	< 25% (M)(5)

References. — (1) Sidhu et al. (1992); (2) Adams & Smith (1985); (3) Giles et al. (1992); (4) Walmsley et al. (2004); (5) Cloned, original from UDFA: `www.udfa.net`

[M] Laboratory measurement
[C] Calculated

B. DOMINANT FORMATION AND DESTRUCTION PATHWAYS FOR DEUTERATED SPECIES

Table B2
Important reactions for species involved in the main pathways of the assorted deuterated species; HDO, D_2O, DCO^+, DCN, CH_2DOH, CHD_2OH and CD_3OH.

Reaction			Rates	Accuracy
$H_2^+ + H_2$	⇒	$H_3^+ + H$	2.10E-09 0.00E+00 0.00E+00	< 25% (M)(1)
$H_2 + h\nu_{CR}$	⇒	$H_2^+ + e^-$	9.30E-01 0.00E+00 0.00E+00	factor 2 (L)(1)
$HDO^+ + H_2$	⇒	$H_2DO^+ + H$	4.07E-11 0.00E+00 0.00E+00	< 25% (M)(1)
$D_2O^+ + H_2$	⇒	$HD_2O^+ + H$	4.07E-11 0.00E+00 0.00E+00	< 25% (M)(1)
$H_2D^+ + O$	⇒	$HDO^+ + H$	6.68E-11 -1.56E-01 -1.41E+00	< 50% (M)(1)
$HD_2^+ + O$	⇒	$D_2^+ + H$	6.68E-11 -1.56E+00 -1.41E+00	< 50% (M)(1)
$H_3^+ + C$	⇒	$CH^+ + H_2$	2.00E-09 0.00E+00 0.00E+00	factor 2 (L)(1)
$CH^+ + H_2$	⇒	$CH_2^+ + H$	1.20E-09 0.00E+00 0.00E+00	< 25% (M)(1)
$CH_2^+ + H_2$	⇒	$CH_3^+ + H$	1.20E-09 0.00E+00 0.00E+00	< 25% (M)(1)
$CH_3^+ + HD$	⇒	$CH_2D^+ + H_2$	1.30E-09 0.00E+00 0.00E+00	(M)(2)
$H_2D^+ + HCN$	⇒	$HDCN^+ + H_2$	1.13E-09 -0.50E+00 0.00E+00	< 25% (M)(1)
$H_2D^+ + HNC$	⇒	$HDCN^+ + H_2$	1.00E-09 -0.50E+00 0.00E+00	factor 2 (L)(1)
$HD_2^+ + HCN$	⇒	$D_2CN^+ + H_2$	1.13E-09 -0.50E+00 0.00E+00	< 25% (M)(1)
$HD_2^+ + HNC$	⇒	$D_2CN^+ + H_2$	1.00E-09 -0.50E+00 0.00E+00	factor 2 (L)(1)
$CH_2 + N$	⇒	HCN + H	3.95E-11 1.67E-01 0.00E+00	< 50% (C)(1)
$CH_2 + N$	⇒	HNC + H	3.95E-11 1.67E-01 0.00E+00	< 50% (C)(1)
$CH + H_2$	⇒	$CH_2 + H$	1.20E-09 0.00E+00 0.00E+00	< 25% (L)(1)
$CH_3^+ + HDO$	⇒	CH_3OHD^+	1.11E-11 -1.70E+00 0.00E+00	(3)
$CH_3^+ + D_2O$	⇒	$CH_3OD_2^+$	1.11E-11 -1.70E+00 0.00E+00	(3)
$CH_2D^+ + H_2O$	⇒	$CH_2DOH_2^+$	1.11E-11 -1.70E+00 0.00E+00	(3)
$CHD_2^+ + H_2O$	⇒	$CHD_2OH_2^+$	1.65E-11 -1.70E+00 0.00E+00	(3)
$CD_3^+ + H_2O$	⇒	$CD_3OH_2^+$	2.20E-11 -1.70E+00 0.00E+00	(3)
$CH_2^+ + H_2$	⇒	$CH_3^+ + H$	1.20E-09 0.00E+00 0.00E+00	< 25% (M)(1)
$CH_3^+ + H_2$	⇒	CH_5^+	3.78E-16 -2.30E+00 2.15E+01	factor 2 (M)(1)
$CH_3^+ + HD$	⇒	$CH_2D^+ + H_2$	1.30E-09 0.00E+00 0.00E+00	(M)(2)
$CH_2D^+ + H_2$	⇒	CH_4D^+	2.00E-14 -1.00E+00 0.00E+00	(M)(2)
$CH_3^+ + D_2$	⇒	$CHD_2^+ + H_2$	6.60E-10 0.00E+00 0.00E+00	(M)(2)
$CHD_2^+ + H_2$	⇒	$CH_3D_2^+$	3.50E-14 -1.00E+00 0.00E+00	(M)(2)
$CD_3^+ + H_2$	⇒	$CH_2D_3^+$	6.30E-14 -1.00E+00 0.00E+00	(M)(2)
$D_3^+ + CH_2$	⇒	$CD_3^+ + H_2$	5.19E-11 -0.50E+00 0.00E+00	factor 2 (L)(1)

References. — (1) Cloned, original from UDFA: `www.udfa.net`; (2) Smith et al. (1982b,a); (3) Roberts et al. (2004)

[M] Laboratory measurement
[C] Calculated
[L] Litterature

Table B3
Most essential formation and destruction pathways for deuterated water; HDO and D_2O.

Reaction			Rates	Accuracy
$H_2DO^+ + e^-$	⇒	HDO + H	2.20E-08 -0.50E+00 0.00E+00	< 25% (M)(1)
$HD_2O^+ + e^-$	⇒	HDO + D	2.20E-08 -0.50E+00 0.00E+00	< 25% (M)(1)
$CHDCO^+ + e^-$	⇒	HDO + C_2	1.00E-07 -0.50E+00 0.00E+00	factor 2 (L)(1)
H_2DO^+ + HCN	⇒	HDO + H_2CN^+	5.47E-10 -0.50E+00 0.00E+00	< 25% (M)(1)
H_2DO^+ + HNC	⇒	HDO + H_2CN^+	5.47E-10 -0.50E+00 0.00E+00	factor 2 (L)(1)
$H_2DO^+ + C_3$	⇒	HDO + C_3H^+	4.00E-10 0.00E+00 0.00E+00	factor 2 (L)(1)
H_2+ OD	⇒	HDO + H	9.33E-14 1.00E+00 1.04E+03	< 25% (M)(1)
HDO	⇒	HDO (ice)		
HDO (ice)	⇒	HDO		
OD (ice) + H (ice)	⇒	HDO (ice)		
OH (ice) + D (ice)	⇒	HDO (ice)		
HDO + HCO^+	⇒	H_2DO^+ + CO	4.20E-10 -0.50E+00 0.00E+00	< 50% (M)(1)
HDO + H_3^+	⇒	$H_2DO^+ + H_2$	1.67E-10 -0.50E+00 0.00E+00	< 25% (M)(1)
HDO + H_3^+	⇒	H_3O^+ + HD	1.67E-10 -0.50E+00 0.00E+00	< 25% (M)(1)
HDO + C^+	⇒	DOC^+ + H	6.00E-10 -0.50E+00 0.00E+00	< 25% (M)(1)
HDO + C^+	⇒	DCO^+ + H	2.97E-10 -0.50E+00 0.00E+00	< 25% (M)(1)
HDO + C^+	⇒	HOC^+ + D	6.00E-10 -0.50E+00 0.00E+00	< 25% (M)(1)
HDO + C^+	⇒	HCO^+ + D	2.97E-10 -0.50E+00 0.00E+00	< 25% (M)(1)
$HD_2O^+ + e^-$	⇒	D_2O + H	2.20E-08 -0.50E+00 0.00E+00	< 25% (M)(1)
HD_2O^+ + HCN	⇒	$D_2O + H_2CN^+$	5.47E-10 -0.50E+00 0.00E+00	< 25% (M)(1)
HD_2O^+ + HNC	⇒	$D_2O + H_2CN^+$	4.95E-10 -0.50E+00 0.00E+00	factor 2 (L)(1)
$HD_2O^+ + C_3$	⇒	$D_2O + C_3H^+$	4.00E-10 0.00E+00 0.00E+00	factor 2 (L)(1)
$D_3O^+ + e^-$	⇒	D_2O + D	2.20E-08 -0.50E+00 0.00E+00	< 25% (M)(1)
$CD_2CO^+ + e^-$	⇒	$D_2O + C_2$	1.00E-07 -0.50E+00 0.00E+00	factor 2 (L)(1)
OD + O_2D	⇒	$D_2O + O_2$	4.00E-11 0.00E+00 0.00E+00	< 25% (L)(1)
OD + OD	⇒	D_2O + O	5.50E-13 1.14E+00 5.00E+01	< 25% (L)(1)
D_2O	⇒	D_2O (ice)		
D_2O (ice)	⇒	D_2O		
$D_2O + C^+$	⇒	DOC^+ + D	6.00E-10 -0.50E+00 0.00E+00	< 25% (M)(1)
$D_2O + C^+$	⇒	DCO^+ + D	2.97E-10 -0.50E+00 0.00E+00	< 25% (M)(1)
$D_2O + H_3^+$	⇒	$HD_2O^+ + H_2$	1.67E-10 -0.50E+00 0.00E+00	< 25% (M)(1)
$D_2O + H_3^+$	⇒	H_2DO^+ + HD	1.67E-10 -0.50E+00 0.00E+00	< 25% (M)(1)
$D_2O + H_3^+$	⇒	$H_3O^+ + D_2$	1.67E-10 -0.50E+00 0.00E+00	< 25% (M)(1)
$D_2O + H^+$	⇒	D_2O^+ + H	8.11E-10 -0.50E+00 0.00E+00	< 25% (M)(1)
$D_2O + H^+$	⇒	HDO^+ + D	8.11E-10 -0.50E+00 0.00E+00	< 25% (M)(1)

References. — (1) Cloned, original from UDFA: `www.udfa.net`

[M] Laboratory measurement

[L] Litterature

Table B4
Most essential formation and destruction pathways for DCO^+.

Reaction			Rates			Accuracy
$H_2D^+ + CO$	⇒	$DCO^+ + H_2$	3.22E-10	0.00E+00	0.00E+00	< 25% (M)(1)
$HCO^+ + D$	⇒	$DCO^+ + H$	1.00E-09	0.00E+00	0.00E+00	(C)(2)
$HD_2^+ + CO$	⇒	$DCO^+ + HD$	3.22E-10	0.00E+00	0.00E+00	< 25% (M)(1)
$D_3^+ + CO$	⇒	$DCO^+ + D_2$	3.22E-10	0.00E+00	0.00E+00	< 25% (M)(1)
$N_2D^+ + CO$	⇒	$DCO^+ + N_2$	8.80E-10	0.00E+00	0.00E+00	< 25% (M)(1)
$DCO_2^+ + CO$	⇒	$DCO^+ + CO_2$	2.47E-10	-0.50E+00	0.00E+00	factor 2 (L)(1)
$DOC^+ + H_2$	⇒	$DCO^+ + H_2$	1.11E-12	0.00E+00	0.00E+00	< 50% (M)(1)
$CH_2D^+ + O$	⇒	$DCO^+ + H_2$	4.10E-11	0.00E+00	0.00E+00	< 25% (M)(1)
$CH_4D^+ + CO$	⇒	$DCO^+ + CH_4$	3.51E-11	-0.50E+00	0.00E+00	< 25% (M)(1)
$C_2HD^+ + O$	⇒	$DCO^+ + CH$	1.67E-11	0.00E+00	0.00E+00	< 25% (M)(1)
$CD + O$	⇒	$DCO^+ + e^+$	2.00E-11	0.40E+00	0.00E+00	< 50% (C)(1)
$DCO^+ + e^-$	⇒	$CO + D$	2.40E-07	0.69E+00	0.00E+00	< 25% (M)(1)
$DCO^+ + SO$	⇒	$DSO^+ + CO$	3.30E-09	-0.50E+00	0.00E+00	factor 2 (L)(1)
$DCO^+ + H$	⇒	$HCO^+ + D$	2.20E-09	0.00E+00	7.69E+02	(C)(2)
$DCO^+ + C$	⇒	$CD^+ + CO$	1.10E-09	0.00E+00	0.00E+00	factor 2 (L)(1)
$DCO^+ + HCN$	⇒	$HDCN^+ + CO$	2.43E-09	-0.50E+00	0.00E+00	< 25% (M)(1)
$DCO^+ + HNC$	⇒	$HDCN^+ + CO$	2.21E-09	0.00E+00	0.00E+00	< 25% (M)(1)

References. — (1) Cloned, original from UDFA: `www.udfa.net`; (2) Adams & Smith (1985)
[M] Laboratory measurement
[C] Calculated
[L] Litterature

Table B5
Most essential formation and destruction pathways for deuterated DCN.

Reaction			Rates	Accuracy
$HDCN^+ + e^-$	⇒	DCN + H	6.17E-08 -0.65E+00 0.00E+00	(1)
$D_2CN^+ + e^-$	⇒	DCN + D	6.17E-08 -0.65E+00 0.00E+00	(1)
HCN + D	⇒	DCN + H	1.00E-10 -0.50E+00 5.00E+02	(2)
NH_2D + CN	⇒	DCN + NH_2	2.76E-12 -1.14E+00 0.00E+00	< 50% (M)(3)
$CHDCN^+ + e^-$	⇒	DCN + CH	1.00E-07 -0.50E+00 0.00E+00	factor 2 (L)(3)
DCO + N	⇒	DCN + O	1.70E-10 0.00E+00 0.00E+00	factor 2 (L)(3)
CHD + N	⇒	DCN + H	1.32E-11 1.67E-01 0.00E+00	< 50% (C)(3)
HDCN + H	⇒	DCN + H_2	1.11E-11 0.00E+00 0.00E+00	factor 2 (M)(3)
$CH_2DCN^+ + e^-$	⇒	DCN + CH_2	6.00E-08 -0.50E+00 0.00E+00	factor 2 (L)(3)
$C_2HD^+ + N$	⇒	DCN + CH^+	8.33E-12 0.00E+00 0.00E+00	< 25% (M)(3)
$C_3DN^+ + H_2$	⇒	DCN + C_2H_2	2.22E-13 0.00E+00 0.00E+00	< 25% (M)(3)
DCN	⇒	DCN (ice)		
DCN (ice)	⇒	DCN		
DCN + H_3^+	⇒	$HDCN^+ + H_2$	1.13E-09 -0.50E+00 0.00E+00	< 25% (M)(3)
DCN + H_3^+	⇒	$H_2CN^+ + HD$	1.13E-09 -0.50E+00 0.00E+00	< 25% (M)(3)
DCN + HCO^+	⇒	$HDCN^+ + CO$	2.43E-09 -0.50E+00 0.00E+00	< 25% (M)(3)
DCN + He^+	⇒	$CN^+ + He + D$	6.90E-09 -0.50E+00 0.00E+00	< 25% (M)(3)
DCN + H^+	⇒	$DCN^+ + H$	5.56E-09 -0.50E+00 0.00E+00	< 25% (M)(3)
DCN + H	⇒	HCN + D	1.00E-10 -0.50E+00 5.00E+02	(2)
DCN + H_3O^+	⇒	$HDCN^+ + H_2O$	5.47E-10 -0.50E+00 0.00E+00	< 25% (M)(3)
DCN + H_3O^+	⇒	$H_2CN^+ + HDO$	5.47E-10 -0.50E+00 0.00E+00	< 25% (M)(3)
DCN + D_3O^+	⇒	$D_2CN^+ + D_2$	1.13E-09 -0.50E+00 0.00E+00	< 25% (M)(3)
DCN + C^+	⇒	$CNC^+ + D$	4.75E-09 -0.50E+00 0.00E+00	< 25% (M)(3)
DCN + C^+	⇒	$C_2N^+ + D$	4.75E-09 -0.50E+00 0.00E+00	factor 2 (L)(3)

References. — (1) Cloned, original from KIDA: `http://kida.obs.u-bordeaux1.fr/`; (2) Schilke et al. (1992); (3) Cloned, original from UDFA: `www.udfa.net`; (4)

[M] Laboratory measurement
[C] Calculated
[L] Litterature

Table B6
Most essential formation and destruction pathways for deuterated CH_3OH; CH_2DOH, CHD_2OH and CD_3OH.

Reaction			Rates	Accuracy
$CH_2DOH_2^+ + e^-$	⇒	$CH_2DOH + H$	7.38E-10 -0.67E+00 0.00E+00	< 25% (M)(1)
$CH_3OHD^+ + e^-$	⇒	$CH_2DOH + H$	7.38E-10 -0.67E+00 0.00E+00	< 25% (M)(1)
$CH_3OD_2^+ + e^-$	⇒	$CH_2DOH + D$	7.38E-10 -0.67E+00 0.00E+00	< 25% (M)(1)
CH_2DOH	⇒	CH_2DOH (ice)		
CH_2DOH (ice)	⇒	CH_2DOH		
$CHD_2OH_2^+ + e^-$	⇒	$CHD_2OH + H$	7.38E-10 -0.67E+00 0.00E+00	< 25% (M)(1)
$CH_2DOHD^+ + e^-$	⇒	$CHD_2OH + H$	7.38E-10 -0.67E+00 0.00E+00	< 25% (M)(1)
$CH_3OD_2^+ + e^-$	⇒	$CHD_2OH + H$	7.38E-10 -0.67E+00 0.00E+00	< 25% (M)(1)
CHD_2OH	⇒	CHD_2OH (ice)		
CHD_2OH (ice)	⇒	CHD_2OH		
$CD_3OH_2^+ + e^-$	⇒	$CD_3OH + H$	7.38E-10 -0.67E+00 0.00E+00	< 25% (M)(1)
$CHD_2OHD^+ + e^-$	⇒	$CD_3OH + H$	7.38E-10 -0.67E+00 0.00E+00	< 25% (M)(1)
$CH_2DOD_2^+ + e^-$	⇒	$CD_3OH + H$	7.38E-10 -0.67E+00 0.00E+00	< 25% (M)(1)
$CHD_2OD_2^+ + e^-$	⇒	$CD_3OH + D$	7.38E-10 -0.67E+00 0.00E+00	< 25% (M)(1)
CD_3OH	⇒	CD_3OH (ice)		
CD_3OH (ice)	⇒	CD_3OH		

References. — (1) Cloned, original from UDFA: `www.udfa.net`
[M] Laboratory measurement

C. LISTING OF OBSERVED DEUTERATED FRACTIONATION RATES IN COLD, DARK, INTERSTELLAR ENVIRONMENTS

Table C1 Listings of observated interstellar deuterated species.

Species	Sources		Spacial scale	Refs	Model
	Class -I	Class O/I	Beam size ["]		
D / H	$< 4.8 \times 10^{-4}$		1.8°	1	$10^{-3} - 10^{-2}$
- -	$2.3 \pm 0.4 \times 10^{-5}$			2	- -
- -	$1.8 - 2.4 \times 10^{-5}$			3	- -
- -	< 0.14			4	
HD / H_2	$0.74 - 8.6 \times 10^{-6}$		30x30	5	$< 10^{-4}$
- -	$6.6 - 70 \times 10^{-7}$			6	- -
- -	5.98×10^{-5}			7	- -
- -	$2.48 - 5.94 \times 10^{-5}$			7	- -
ND / NH		0.3 - 1.0	41	8	$10^{-4} - 10^{0}$
OD / OH	$< 2.5 \times 10^{-3}$		1.8°	9	$10^{-2} - 10^{0}$
CCD / CCH	0.01		33	10	$10^{-3} - 10^{-2}$
- -	0.045		33	10	- -
- -	0.01 - 0.18		20	11	- -
D_2O / H_2O		5×10^{-5}	1.5x1.5	12	$< 10^{-5} - 10^{-3}$
D_2S / H_2S	< 0.264		31 [b]	13	$10^{-4} - 10^{-2}$
DCN / HCN	0.008-0.015			14	$10^{-3} - 10^{-1}$
- -	0.012 - 0.11			15	- -
DCO^+ / HCO^+	0.013 - 0.023		20	11	$10^{-2} - 10^{0}$
- -	0.02 - 0.18		20	16	- -
- -	0.021		7x5	17	- -
- -	0.006 - 0.04		25-57	18	- -
- -	0.045 ± 0.014		30-96	19	- -
- -	0.007 - 0.081			15	- -
- -	< 0.03			4	- -
- -		0.0006		14	$10^{-4} - 10^{-2}$
- -		6.1×10^{-4}	10-30	20	- -
- -		0.007 - 0.011	10-30	20	- -
DNC / HNC	0.015 - 0.03		20	11	$10^{-3} - 10^{-1}$
- -	0.02 - 0.09		~ 20	21	- -
- -	0.008 - 0.122		17-20[a]	22	- -
H_2D^+/ H_3^+		$< 3 \times 10^{-3}$	13[b]	23	$10^{-4} - 10^{-2}$
HDO / H_2O	0.07	≥ 0.01	10-30	24	$10^{-3} - 10^{-1}$
- -	< 0.002	0.03	10-33	25	- -
- -		2.94×10^{-2}	1.5x1.5	26	$10^{-2} - 10^{-1}$
- -		$< 6 \times 10^{-4}$	3.1 x 2.5	27	$10^{-4} - 10^{-2}$
HDO / H_2O (solid)		0.005 - 0.02		28	$10^{-3} - 10^{-1}$
- -		$10^{-3} - 10^{-2}$		29	- -
HDS / H_2S	0.10 ± 0.05		20	11	$10^{-2} - 10^{-1}$
N_2D^+ / N_2H^+	0.08 - 0.35		20	16	$10^{-2} - 10^{0}$
- -	0.03 - 0.04		26.4 [a]	30	- -
- -	0.017 - 0.052		$\sim$30	31	- -
- -	0.04 - 0.44		11 [a]	32	- -
- -	0.11		44	33	- -
- -	0.03 - 0.1		10-20	34	- -
- -	0.11 ± 0.03		18 [a]	35	- -
- -	~ 0.1		9-26[a]	36	- -
- -		0.042 - 0.271	11-16	37	$10^{-4} - 10^{-2}$
- -		0.005 - 0.014	11-26 [a]	38	- -
- -		0.029 - 0.27		39	- -
- -		0.015	9-26[a]	40	- -
D_2CO / H_2CO	0.143 ± 0.019		27 [a]	41	$10^{-3} - 10^{-2}$
- -	0.01 - 0.1		17	42	- -
- -	2.94×10^{-1}		20-60	43	- -
- -	≤ 0.07		22	44	- -
- -		0.046 - 0.44	10-30	45	$10^{-5} - 10^{-3}$
- -		0.02 - 0.4		46	- -
- -		0.01 - 0.04	20-60	47	- -
D_2CS / H_2CS	0.333			48	$10^{-3} - 10^{-1}$
HDCO / H_2CO	0.014 - 0.015		20	11	$10^{-3} - 10^{-1}$
- -	1.4×10^{-1}		20-60	43	- -
- -	0.005-0.11		33	10	
- -	0.107 ± 0.015		27 [a]	49	- -
- -	0.01 - 0.14		22	44	- -
- -		0.094 - 1.7	10-30	45	$10^{-4} - 10^{-2}$
- -		~ 0.15		50	- -
- -		0.01 - 0.07	10-80	47	- -
- -		0.14	20-60	43	- -
- -		0.006		14	- -

Species	Sources		Spacial scale	Refs	Model
	Class -I	Class O/I	Beam size ["]		
HDCS / H_2CS	0.020± 0.005		>60	51	$10^{-2} - 10^{-1}$
- -	0.333			48	$10^{-2} - 10^{-1}$
ND_3 / NH_3	$\sim 8 \times 10^{-4}$		25	52	$< 10^{-5} - 10^{-3}$
- -	0.024 - 0.033		22 [b]	53	- -
- -		9.35×10^{-4}	25	54	$< 10^{-5} - 10^{-4}$
NH_2D / NH_3	0.02 - 0.1		20	16	$10^{-3} - 10^{-1}$
- -	0.025 - 0.18		18	55	- -
- -	0.10 - 0.28		22 [b]	54	$10^{-4} - 10^{-2}$
- -	< 0.02		20	11	- -
- -	0.1	0.06	22	44	- -
- -	0.1 - 0.8	< 0.1	7	56	- -
- -		0.0028 - 0.13	~ 20	57	$10^{-5} - 10^{-3}$
- -		0.04 - 0.33	37	58	$10^{-2} - 10^{-1}$
- -		0.06	20-60	43	- -
NHD_2 / NH_3	5×10^{-3}		22	43	$10^{-4} - 10^{-1}$
- -	0.05 - 0.22		22 [b]	54	- -
- -		0.02 - 0.4		50	$< 10^{-5} - 10^{-3}$
C_3HD / C_3H_2	0.05 - 0.15		1.7' [b]	59	$10^{-3} - 10^{-1}$
C_4D / C_4H	0.0043		1.7' [b]	60	$10^{-3} - 10^{-1}$
- -	0.0043-0.018		17-28	61	$10^{-3} - 10^{-2}$
C_4HD / C_4H2		0.03	17-28	61	$10^{-3} - 10^{-1}$
CD_3OH/ CH_3OH		0.014± 0.014	15	62	$< 10^{-5} - 10^{-2}$
CH_2DCCH / CH_3CCH	0.081 - 0.170		40-60	63	$10^{-3} - 10^{-1}$
- -	0.05 - 0.06		27[a]	64	- -
- -	0.07 - 0.10		40	65	- -
CH_2DCN / CH_3CN		≥ 0.005	27 [a]	66	$10^{-2} - 10^{-1}$
CH_2DOH / CH_3OH	0.05 - 0.30		40-60	63	$10^{-1} - 10^{1}$
- -		0.43 - 0.65	10-30	45	$10^{-3} - 10^{-1}$
- -		0.90 ± 0.3	11-30	67	$10^{-1} - 10^{0}$
- -		0.37± 0.38	17-28	61	$10^{-1} - 10^{0}$
- -		0.05 - 0.30		68	- -
CH_3OD/ CH_3OH	≤ 0.1		20	11	
- -		0.016 - 2.5	10-30	45	
- -		0.04 ± 0.02	11-30	67	$10^{-2} - 10^{0}$
CHD_2OH/ CH_3OH		0.2± 0.1	11-30	67	$10^{-3} - 10^{0}$
DC_3N / HC_3N	0.05 - 0.1		38-52 [a]	69	$10^{-3} - 10^{-1}$
- -		0.031 ± 0.011	17-28	61	$10^{-4} - 10^{-2}$
DC_5N / HC_5N	0.006-0.016		1.4 [a]	70	$10^{-3} - 10^{-2}$
$DCOOCH_3$ / $HCOOCH_3$	0.02 - 0.06			71	$10^{-3} - 10^{-1}$
- -	~ 0.15		9-33	72	- -

References. — (1) Cesarsky et al. (1973); (2) Hébrard (2006); (3) Rogers et al. (2007); (4) Heiles et al. (1993); (5) Lacour et al. (2005); (6) Snow et al. (2008); (7) Balashev et al. (2010); (8) Bacmann et al. (2010); (9) Allen et al. (1974); (10) Millar et al. (1989); (11) van Dishoeck et al. (1995); (12) Butner et al. (2007); (13) Vastel et al. (2003); (14) Parise et al. (2007); (15) Lis et al. (2002a); (16) Tiné et al. (2000); (17) Goicoechea et al. (2009); (18) Anderson et al. (1999); (19) Butner et al. (1995); (20) Parise et al. (2009); (21) Hirota et al. (2003); (22) Hirota et al. (2001); (23) Stark et al. (1999); (24) Liu et al. (2011); (25) Parise et al. (2005); (26) Butner et al. (2007); (27) Jørgensen & van Dishoeck (2010); (28) Parise et al. (2003); (29) Teixeira et al. (1999); (30) Miettinen et al. (2009); (31) Chen et al. (2010); (32) Crapsi et al. (2005); (33) Fontani et al. (2008); (34) Friesen et al. (2010); (35) Belloche et al. (2006); (36) Crapsi et al. (2004); (37) Emprechtinger et al. (2009); (38) Alonso-Albi et al. (2010); (39) Emprechtinger et al. (2007); (40) Fontani et al. (2006); (41) Bergman et al. (2011); (42) Bacmann et al. (2003); (43) Turner (1990); (44) Roueff et al. (2000); (45) (Parise et al. 2006); (46) Loinard et al. (2002); (47) Roberts & Millar (2007); (48) Marcelino et al. (2005); (49) Bergman et al. (2011); (50) Loinard et al. (2003); (51) Minowa et al. (1997); (52) Lis et al. (2002b); (53) Roueff et al. (2005); (54) van der Tak et al. (2002); (55) Saito et al. (2000); (56) Busquet et al. (2010); (57) Shah & Wootten (2001); (58) Hatchell (2003); (59) Bell et al. (1988); (60) Turner (1989); (61) Sakai et al. (2009); (62) Parise et al. (2004); (63) Markwick et al. (2005); (64) Gerin et al. (1992a); (65) Markwick et al. (2002); (66) Gerin et al. (1992b); (67) Parise et al. (2002); (68) Bacmann et al. (2007); (69) Howe et al. (1994); (70) MacLeod et al. (1981); (71) Margulès et al. (2010); (72) Demyk et al. (2010)

[a] Half-power beam width (HPBW)

[b] Full-width half-maximum (FWHM)

[c] LWRS